AGU PUBLICATIONS

JGR

Journal of Geophysical Research: Solid Earth

RESEARCH ARTICLE
10.1002/2017JB014424

Key Points:
- Elastic vertical displacements are inverted to infer change in total water storage in mountain ranges in the western U.S. from 2006 to 2017
- Sierra Nevada uplift during severe drought from 2012 to 2015 is primarily solid Earth's elastic response to water loss in the Sierra Nevada
- More water in the ground in California's mountains is lost during drought and gained during heavy precipitation than in hydrology models

Supporting Information:
- Supporting Information S1

Correspondence to:
D. F. Argus,
donald.f.argus@jpl.nasa.gov

Citation:
Argus, D. F., Landerer, F. W., Wiese, D. N., Martens, H. R., Fu, Y., Famiglietti, J. S., … Watkins, M. M. (2017). Sustained water loss in California's mountain ranges during severe drought from 2012 to 2015 inferred from GPS. *Journal of Geophysical Research: Solid Earth*, *122*, 10,559–10,585. https://doi.org/10.1002/2017JB014424

Received 10 MAY 2017
Accepted 20 NOV 2017
Accepted article online 24 NOV 2017
Published online 26 DEC 2017

Sustained Water Loss in California's Mountain Ranges During Severe Drought From 2012 to 2015 Inferred From GPS

Donald F. Argus[1], Felix W. Landerer[1], David N. Wiese[1], Hilary R. Martens[2], Yuning Fu[3], James S. Famiglietti[1], Brian F. Thomas[4], Thomas G. Farr[1], Angelyn W. Moore[1], and Michael M. Watkins[1]

[1]NASA Jet Propulsion Laboratory, California Institute of Technology, Pasadena, CA, USA, [2]Department of Geosciences, University of Montana, Missoula, MT, USA, [3]School of Earth, Environment, and Society, Bowling Green State University, Bowling Green, OH, USA, [4]Department of Geology and Environmental Science, University of Pittsburg, Pittsburgh, PA, USA

Abstract Drought struck California during 7 of the 9 years from 2007 to 2015, reducing the state's available water resources. Pumping of Central Valley groundwater has produced spectacular land subsidence. Uplift of the adjacent Sierra Nevada mountains has been proposed to be either tectonic uplift or solid Earth's elastic response to unloading of Central Valley groundwater. We find that of the 24 mm of uplift of the Sierra Nevada from October 2011 to October 2015, just 5 mm is produced by Central Valley groundwater loss, less than 2 mm is tectonic uplift, and 17 mm is solid Earth's elastic response to water loss in the Sierra Nevada. We invert GPS vertical displacements recording solid Earth's elastic response to infer changes in water storage across the western U.S. from January 2006 to October 2017. We find water changes to be sustained over periods of drought or heavy precipitation: the Sierra Nevada lost 15 ± 19 km^3 of water during drought from October 2006 to October 2009, gained 18 ± 14 km^3 of water during heavy precipitation from October 2009 to October 2011, and lost 45 ± 21 km^3 of water during severe drought from October 2011 to October 2015 (95% confidence limits). Such large changes are not in hydrology models: snow accumulation in October is negligible and long-term soil moisture change is small. We infer that there must be large loss of either deep soil moisture or groundwater in river alluvium and in crystalline basement in the Sierra Nevada. The results suggest there to be parching of water in the ground during the summer of years of drought and seeping of melting snow into the Sierra Nevada in the spring of years of heavy precipitation.

1. Introduction

Rain and snowfall in California vary strongly by year. While precipitation was heavy in 2011 and 2017, California suffered a severe drought from 2012 to 2015 (Griffin & Anchukaitis, 2014; Swain, 2015). Precipitation during the 4 years was 50% of its historical average, with rain and snowfall being particularly low in the southern Sierra Nevada in 2014 and 2015 (California Data Exchange Center (CDEC), 2017a; PRISM Climate Group, 2017). California's rainy season starts in October and ends in May, before the dry season begins in June and lasts through September (Figure 1a). We therefore refer to water years: water year 2015 starts 1 October 2014 and ends 30 September 2015.

Solid Earth deforms in elastic response to changes in the surface load of water, snow, ice, and atmosphere. Earth's elastic response is nearly known and specified by Green's functions (Farrell, 1972) that are not very sensitive to Earth's rheologic structure (Chanard et al., 2014; Wahr et al., 2013). Elastic vertical displacement of Earth's surface naturally resolves a mass load with high fidelity because displacement decreases rapidly with distance from a surface load. For example, for a disk with a radius of 7 km, the vertical displacement at 20 km from the load center is half that at 10 km from the load center (Argus, Fu, et al., 2014, Figure 1). Therefore, measurements of vertical land displacement at closely spaced GPS sites can be used to infer changes in the total mass load. In this study, we invert vertical displacements at 1,276 GPS sites for change in mass as a function of location and time in the western U.S. from January 2006 to October 2017. We follow the general inversion method of three prior studies (Argus, Fu, et al., 2014; Borsa et al., 2014; Fu et al., 2015) (see also Ouellette et al., 2013; Tregoning et al., 2009).

In most of the western U.S., vertical land displacement records solid Earth's elastic response to the loading of snow and water. Earth's surface subsides in the fall and winter when loaded by snow and rain. The ground

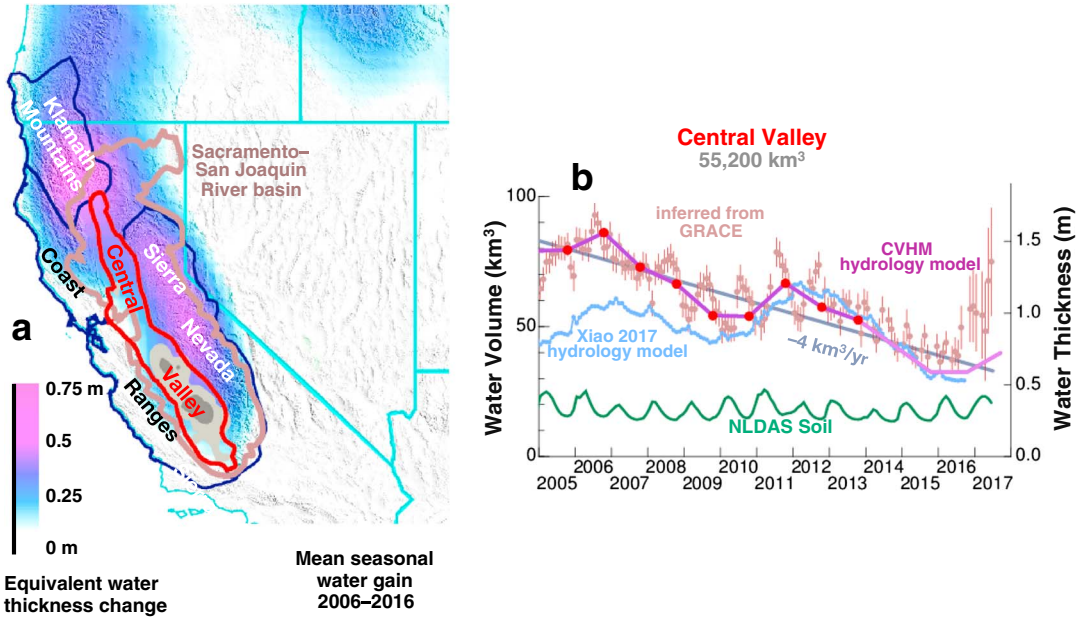

Figure 1. (a) Mean seasonal water gain inferred from GPS (blue/violet color gradations) is plotted with the locations of four physiographic provinces: the Central Valley, the Sierra Nevada, the California Coast Ranges, and the Klamath mountains (Thelin & Pike, 1991). The Sacramento-San Joaquin River basin (pink-gray outline) is also shown. The mean seasonal water gain is the increase in equivalent water thickness from 1 October to 1 April taken from a sinusoid fit to total water change inferred from GPS. (b) Central Valley groundwater change is compared between the hydrology model of Faunt et al. (2015), the hydrology model of Xiao et al. (2017) and that inferred from GRACE. GRACE error bars are 95% confidence limits. Soil moisture in NLDAS-Noah is also plotted. The Central Valley Hydrologic Model (CVHM) (Faunt et al., 2015) is a comprehensive model simulating surface water flow, irrigation, precipitation, and evapotranspiration. We construct an a priori model of groundwater change in the Central Valley (violet curve) on the basis of the Central Valley Hydrologic Model (CVHM) (Faunt, 2009; Faunt et al., 2015) from 2006 to 2013 and the water-balance model of Xiao et al. (2017) from 2013 to 2016. Groundwater change is inferred from GRACE following the method of Famiglietti et al. (2011): A composite hydrology model consisting of snow water equivalent in SNODAS, soil moisture in NLDAS-Noah, and reservoir surface water in CDEC is removed from the GRACE estimate of change in total water in the Sacramento-San Joaquin River basin. This GRACE estimate is corrected for leakage by a 1.25 scaling factor (Wiese et al., 2016) calculated on the basis of the spatial distribution of seasonal oscillations in the Community Land Model (Lawrence et al., 2011).

rises in the spring and summer when the snow melts and the resulting water runs off or evaporates. Earth's surface at the top of an aquifer, however, responds in an opposite manner. An aquifer expands as water fills the porous gravel, sand, and silt in the aquifer, causing Earth's surface to rise. Earth's surface rises in the fall and winter when the aquifer is recharged with water and subsides in the spring and summer when groundwater is withdrawn from the aquifer. Thus, Earth's porous response to groundwater is opposite to Earth's elastic response to the loading of water and snow. Whereas GPS sites moving in elastic response to changes in the load of snow and water attain their maximum height at the end of summer, GPS sites on top of aquifers attain their maximum height at the end of winter. Aquifers also have an elastic response, but it is in most places 10 to 100 times smaller than the porous response.

Aquifers are readily identified on the basis of geology (a deep sedimentary basin), the location of groundwater pumping wells, fast land subsidence caused by excessive groundwater pumping, and the time of year of the maximum height of Earth's surface. In the western U.S., the largest aquifer is the Central Valley (700 km × 70 km), which is composed of the Sacramento Valley (the northern half of the Central Valley) and the San Joaquin Valley (the southern half). The Los Angeles Basin, the Santa Clara Basin south of San Francisco, and several groundwater basins in western Utah are the next largest aquifers.

In this study we first omit GPS sites recording solid Earth's porous response to groundwater changes or affected by volcanic activity, next remove elastic deformation in response to known changes in surface water in artificial reservoirs and to changes in atmospheric mass, then remove viscous deformation in response to unloading of the ice sheets 15,000 to 5,000 years ago, and finally determine change in total mass as a function

of location while setting groundwater change in Central Valley to an a priori model constructed on the basis of conventional water-balance measurements. Central Valley groundwater change is set to an a priori model because there are few or no GPS sites recording Earth's elastic response there. If we were to not set Central Valley groundwater change to an a priori model, we would find water change inferred there to be poorly constrained (and to depend on extrapolation of Earth's elastic response from the adjacent Sierra Nevada and California Coast Ranges). While Central Valley groundwater change in the water-balance models may be quite uncertain, we show (in section 6) that our estimates of water change adjacent to the Central Valley depend weakly on what we assume Central Valley groundwater change to be. We then thoroughly analyze the estimates of water change inferred from GPS and place them in the context of precipitation, hydrology models, and Gravity Recovery and Climate Experiment (GRACE) gravity data.

2. Prerequisites

2.1. Proposed Causes of Sierra Nevada Uplift

The southern Sierra Nevada is observed with GPS to have risen at a mean rate of about 1.5 mm/yr from January 2006 to December 2016. This rise is, however, not steady. The Sierra Nevada rises during periods of drought and subsides during years of heavy precipitation. Because there is no snow loading on the solid Earth in October, we quantify vertical displacement of the Sierra Nevada from October to October. The Sierra Nevada rose 9 mm during drought from October 2006 to October 2009, subsided 7 mm during heavy precipitation from October 2009 to October 2011, rose 24 mm during drought from October 2011 to October 2015, and subsided 12 mm from October 2015 to October 2017.

Two causes have been proposed to cause Sierra Nevada uplift. Hammond et al. (2016, 2012) maintain the uplift to be tectonic and associated with normal slip along the Sierra Nevada frontal fault (on the east side of the mountain range). Amos et al. (2014) maintain uplift of the Sierra Nevada to be solid Earth's elastic response to unloading of Central Valley groundwater. In this study, we demonstrate that these two phenomena generate less than half the observed uplift of the Sierra Nevada.

2.2. Sierra Nevada Elastic Uplift Produced by Unloading of Central Valley Groundwater

Groundwater pumping in the San Joaquin Valley has dramatically reduced the volume of groundwater there since 1984 (Famiglietti et al., 2011; Faunt, 2009; Scanlon et al., 2012), causing parts of the valley to subside more than 1 m since 2006 (Farr & Liu, 2014; Faunt et al., 2015; Sneed et al., 2013). Using the rock mechanic formula of Jaeger et al. (2007) for a homogeneous, nongravitating half-space, Amos et al. (2014) conclude that unloading of Central Valley groundwater produces elastic uplift of the Sierra Nevada at "1–3 mm/yr" (the value quoted in their abstract), accounting for all of the observed Sierra Nevada uplift. However, maximum uplift in Amos et al.'s calculation (in their Figure 2) is just 1.65 mm/yr at the load center and 1 mm /yr at the western margin of the Sierra Nevada. The model of Amos et al. (2014) is simple: they assume Central Valley groundwater loss to occur at a steady 4 km^3/yr (Famiglietti et al., 2011) and to be evenly distributed over a rectangular region 450 km in length and 60 km in width.

In this study, we determine solid Earth's elastic response to unloading of Central Valley groundwater using Green's functions (Wang et al., 2012) for a gravitating, spherical, stratified Earth calculated assuming the preliminary reference Earth model (PREM) (Dziewonski & Anderson, 1981) (Figure S1 in the supporting information). We also adapt a more exact description of Central Valley groundwater change as a function of time from 2006 to 2016 and of location in the Sacramento and San Joaquin Valleys. We find unloading of groundwater from primarily the San Joaquin Valley produces elastic uplift of the western margin of the southern Sierra Nevada at just 0.6 mm/yr, explaining 40% of the mean uplift from 2006 to 2016. We next present the specifics of our model. In section 6, we investigate models intermediate between ours and Amos et al.'s (2014) to ascertain the cause of the big difference between the two studies. We find that changing the formulation from a nongravitating half-space to a gravitating sphere reduces solid Earth's elastic response by a factor of 2.5.

In our a priori model, we set total groundwater change in Central Valley equal to the Central Valley Hydrologic Model (CVHM) from 2006 to 2013 (Faunt et al., 2015) and to the water-balance model of Xiao et al. (2017) from 2013 to 2016 (Figure 1b). CVHM is a comprehensive aquifer model constructed using conventional measurements of surface water delivery and groundwater levels. Because the established CVHM model ends in 2013,

we update with the Xiao et al. (2017) water-balance model. A total of 32 km^3 of groundwater is lost during drought from October 2006 to October 2009, 12 km^3 of groundwater is gained during heavy precipitation from October 2009 to October 2011, and 34 km^3 of groundwater is lost during drought from October 2011 to October 2015.

We infer the distribution of groundwater loss from CVHM and vertical land motion. Faunt (2009, Figure B9) estimate that groundwater loss from 1962 to 2002 has occurred nearly entirely in the Tulare Basin (the southern half of the San Joaquin Valley) at 2 km^3/yr. Vertical land displacements support the premise that most groundwater loss from 2006 to 2016 also occurred in the Tulare Basin (Farr & Liu, 2014; Faunt et al., 2015; Sneed et al., 2013) (Figures 2a and S2). GPS and interferometric synthetic aperture radar (InSAR) identify a broad 80 km × 50 km area within the San Joaquin Valley to be subsiding at faster than 10 mm/yr. A second 80 km × 50 km region of the Tulare Basin is observed to be subsiding at 50–300 mm/yr. The Tulare Basin is subsiding rapidly because groundwater is being excessively pumped and because clay lenses in sedimentary layers such as the Corcoran Clay are collapsing, causing greater compaction in response to groundwater withdrawal. In our a priori model, we assume all groundwater change to occur inside the 10 mm/yr land subsidence contour, we take groundwater change inside the 50 mm/yr contour to be twice as fast as inside the 10 mm/yr contour, and we assume groundwater change inside the 100 mm/yr contour to be 3 times as fast as inside the 10 mm/yr contour (Figure 2b). Thus, the mean rate of groundwater loss ranges from 0.42 m/yr (black Zs, area shaded red) at the center of Tulare Basin, to 0.28 m/yr (blue Ys, shaded light red) in areas subsiding fast, and to 0.14 m/yr (red Xs, shaded yellow) in the remainder of San Joaquin Valley and a small 30 km × 20 km area in the Sacramento Valley near Davis.

We determine solid Earth's elastic response to groundwater change in the a priori model using Green's functions for a gravitating, spherical, stratified Earth for PREM (Wang et al., 2012). The pixels (Xs in Figure 2c) are at 1/8° intervals of latitude and longitude. Each is approximated by a disk with a radius of 7 km. We first calculate the elastic response for total groundwater loss at a steady 4 km^3/yr (with groundwater loss distributed as in Figure 2b). Elastic uplift is predicted to be a maximum of 2.4 mm/yr near the center of Tulare Basin (where GPS sites record solid Earth's porous response) and predicted to decrease to about 0.7 mm/yr at the western margin of the southern Sierra Nevada and to about 0.8 mm/yr at the eastern margin of the southern California Coast Ranges (Figure 2c).

We next calculate elastic vertical displacements for the CVHM/Xiao series of groundwater change as a function of time (as in Figure 1b), with the same distribution of groundwater change across San Joaquin Valley (as in Figure 2b). GPS sites in the western Sierra Nevada are predicted to rise 5 mm during drought from October 2006 to October 2009, subside 2 mm during heavy precipitation from October 2009 to October 2011, and rise 5 mm during drought from October 2011 to October 2015 (Figure 3, green curve, and Figure S3). Residual uplift (Figure 3, pink dots) is calculated by subtracting the predicted elastic displacement (green curve) from the observed (blue dots). Residual uplift during drought from October 2011 to October 2015 is 18–23 mm at GPS sites in the western Sierra Nevada and 15–20 mm at GPS sites in the eastern Coast Ranges. In section 5, we attribute this residual uplift during drought from October 2011 to October 2015 to water loss in the Sierra Nevada and Coast Ranges.

There is substantial uncertainty in the a priori model of the temporal evolution and spatial distribution of Central Valley groundwater change. In section 6, we demonstrate that the changes in total water storage that we infer for the mountain ranges adjacent to the Central Valley do not depend strongly on what we assume the groundwater change in Central Valley to be.

2.3. Slow Tectonic Uplift of the Sierra Nevada

Geologic observations from radiometric dating, river incision rates, physical uplift models, and paleoseimology limit tectonic uplift of the Sierra Nevada to be less than 0.5 mm/yr. The timing of Sierra Nevada uplift is controversial. On the basis of the progressive tilt of sedimentary layers, Unruh (1991) infers the crest of the Sierra Nevada to have risen 2,200 m since 5 Ma, yielding an average rate of 0.44 mm/yr. In contrast, Mulch et al. (2006, 2008) and Cassel et al. (2009) maintain on the basis of hydrogen isotopes that the Sierra Nevada mountains attained their present elevation by 30 Ma, suggesting their present uplift rate to be negligible. River incision rates over the past 4 Ma range from 0.1 to 0.4 mm/yr (Wakabayashi, 2013). The study of Stock et al. (2004) maintains that river incision rates have slowed, from 0.3 mm/yr from 3 to 1.5 Ma, to

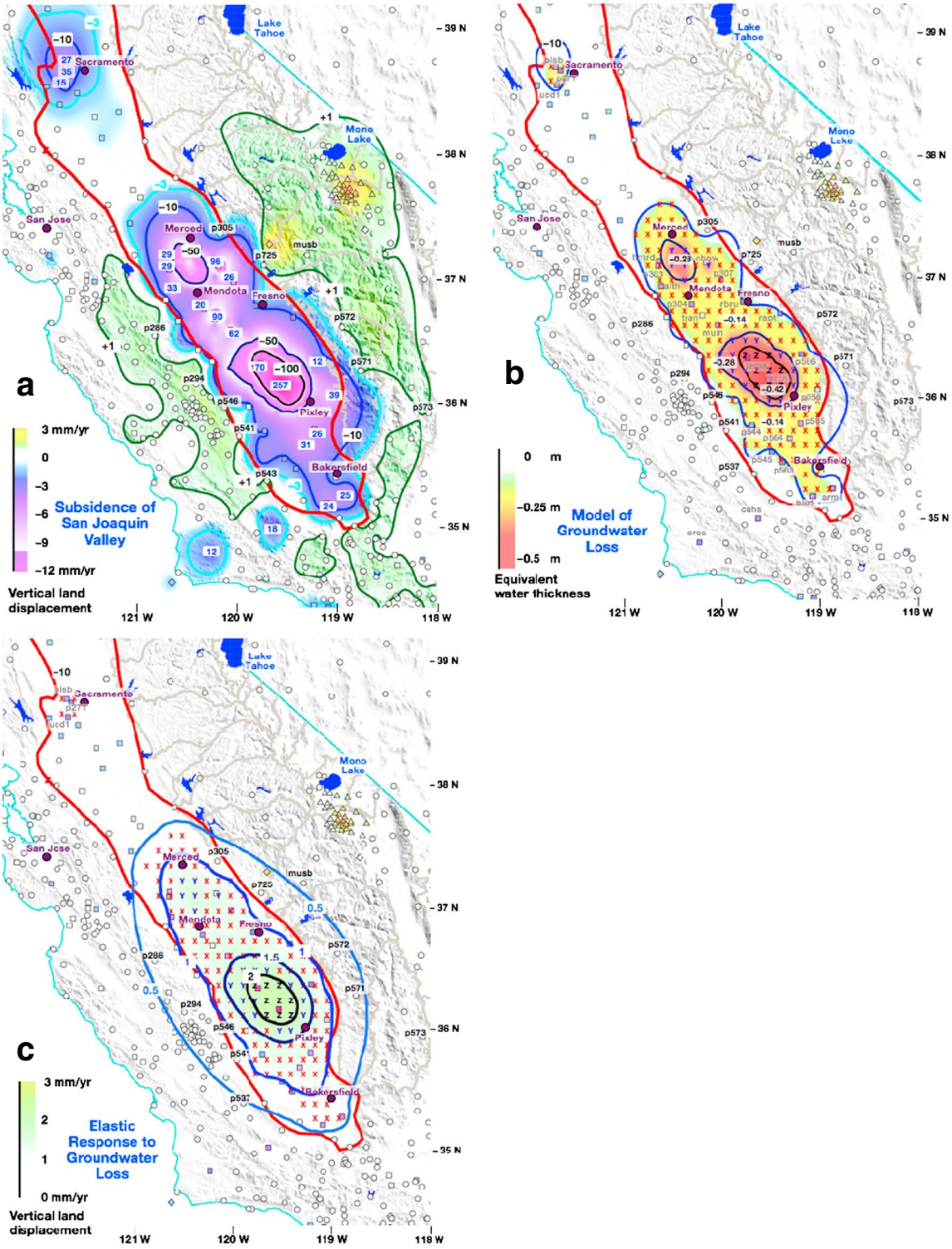

Figure 2. (a) Mean rate of vertical motion taken to be the mean of GPS rates from 2006 to 2016 (this study) and InSAR rates from 2007 to 2010 (Farr & Liu, 2014). Contours are at +1 mm/yr, −3 mm/yr, −10 mm/yr, −50 mm/yr, and −100 mm/yr. Blue numerals show the location of GPS sites and give subsidence rates in mm/yr. (b) Mean rate of decrease in equivalent groundwater thickness from 2006 to 2016 in our a priori model. The Xs, Ys, and Zs are the 1/8° water elements in the model. The red Xs, blue Ys, and black Zs are inside, respectively, the −10 mm/yr, −50 mm/yr, and −100 mm/yr subsidence contours and have water thickness decreases of −0.14 m/yr, −0.28 m/yr, and −0.42 m/yr. (c) Mean rate of uplift from 2006 to 2016 in elastic response to groundwater loss in the model. Contours are at 0.5 mm/yr, 1 mm/yr, 1.5 mm/yr, and 2 mm/yr. Circles are GPS sites recording elastic response to mass change and inverted for water storage change, squares are sites recording porous response to aquifers; triangles are sites affected by volcanoes, and diamonds are sites omitted due to other interfering phenomena. If groundwater loss in the model were distributed evenly across the Central Valley, elastic uplift in the southern Sierras would be predicted to be smaller.

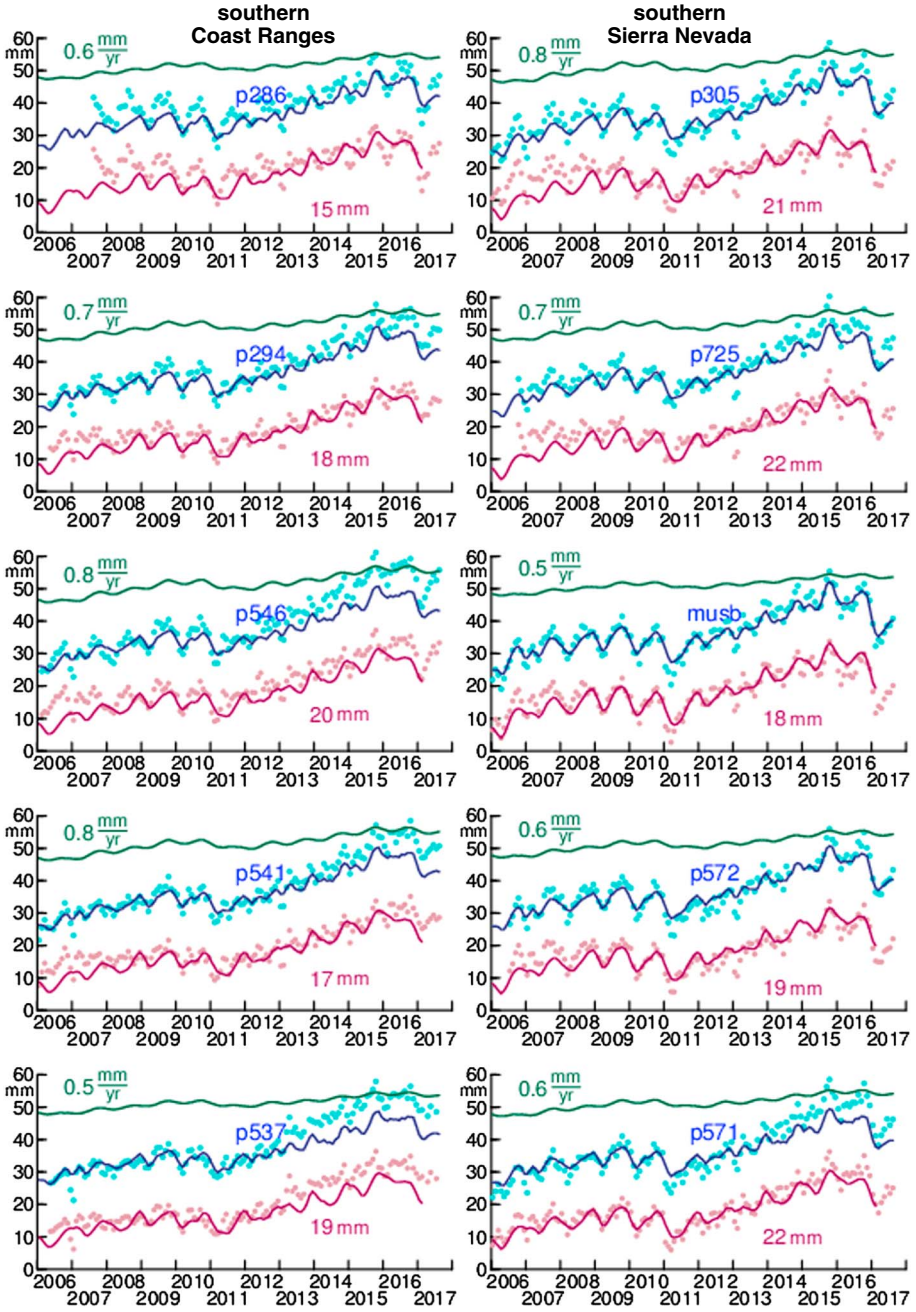

Figure 3. Vertical displacement of GPS sites in the (left column) southern Coast Ranges and the (right column) southern Sierra Nevada. Vertical displacement produced by groundwater change in Central Valley (green) is subtracted from vertical displacement observed with GPS (light blue dots) to obtain residual vertical displacement (pink dots). The mean rate of uplift from 2006 to 2016 produced by Central Valley groundwater change (given in green numerals) is 0.5–0.8 mm/yr. Residual uplift during severe drought from October 2011 to October 2015 (given in maroon numerals) is 15–22 mm and is attributable to water loss in the Coast Ranges and Sierra Nevada. Vertical displacement calculated from water changes in our preferred constrained model (navy curve) approximately fits the GPS data. Vertical displacement calculated from water change in the unconstrained model approximately fits the data corrected for the a priori model of groundwater change in Figure 2c (that the model was fit to). The locations of the GPS sites are shown in Figure 2.

0.03 mm/yr from 1.5 Ma to the present. On the other hand, Gabet (2014) argues that river incision rates inferred from geomorphic interpretation of more than 500 m of uplift (i.e., those in Wakabayashi and in Stock et al.) are unfounded. In a thermodynamic model of delamination of the arclogite (mantle) root of

the Sierra Nevada, Saleeby et al. (2013, Figure 4) have the Sierra Nevada rising 1,000 m in 7 Ma, yielding a rate of 0.14 mm/yr. On the basis of paleoseismic dating of several sedimentary surfaces less than 125 ka, Le et al. (2007) estimate the normal slip on the Sierra Nevada frontal fault to be 0.2–0.3 mm/yr. Thus, the four types of geologic evidence suggest the present tectonic uplift rate of the Sierra Nevada to be between 0 and 0.45 mm/yr. On the basis of convergence rates perpendicular to the San Andreas fault system deduced from the Pacific-Sierra Nevada plate angular velocity, Argus and Gordon (2001) infer that the California Coast Ranges must have been rising for at least the past 4 Ma to attain their present elevation of 1,000 m, yielding an upper limit on the uplift rate of 0.25 mm/yr.

3. Data and Methods

3.1. Determining Vertical Land Displacements Using GPS

The GPS position-time series in this study are primarily from Jet Propulsion Laboratory's (JPL) reprocessed GPS solution (Desai et al., 2011), consisting of satellite orbits, clocks, and site positions from 1991 to the present. This reprocessed solution incorporates satellite phase center variations (igs08.atx) (Schmid et al., 2010) and improved solar radiation models (Sibthorpe et al., 2010). On each day JPL first determines orbits of 24 satellites and positions of 80 sites on Earth's surface. Solid Earth tides, the pole tide, and elastic displacements produced by oceanic tides are corrected for following the International Earth Rotation Service (IERS) standards (Petit & Luzum, 2010). The 1,576 GPS series in this study are next determined using JPL's orbits, clocks, GIPSY software, and precise point positioning technique (Zumberge et al., 1997). JPL determined 1,160 of the 1,576 GPS series. Nevada Geodetic Laboratory determined the remaining 416 GPS series (Blewitt et al., 2013).

We fit each of the 1,576 GPS series with a position, a velocity, a sinusoid with a period of 1 year, and offsets when and where needed (following the methods of Argus et al., 2010, Appendix B). In general, we solve for an offset if an estimated offset is greater than 8 mm in the vertical or 4 mm in the horizontal. The threshold value for solving for an offset is slightly smaller if it is at the time of a logged antenna substitution. We solve for a total of 335 offsets, consisting of 31 offsets at the time of logged antenna substitutions, 156 offsets of unknown cause (possibly at the time of unlogged antenna substitutions), and 148 coseismic offsets.

We took care to be sure that the displacements that we assemble record solid Earth's elastic response. We take 1 January 2011 as the reference time that we specify vertical displacements relative to. The date 1 January 2011 is near the middle of the time period that we have GPS data for. For offsets before 1 January 2011, we deleted all the data before the offset; for offsets after 1 January 2011, we deleted all the data after the offset. At 26 GPS sites, we delete anomalous positions caused by snow on antennas or reflections off of snow; these outlying positions are readily identified by high scatter of tens of millimeters for 1 to 3 months during the snow season. The final set of position-time series has no significant offsets and every series passes through or near 1 January 2011. At each GPS site, we then calculate the mean vertical displacement each month relative to the model value on 1 January 2011 (with the model being the position, velocity, and sinusoid). These mean monthly vertical displacements relative to 1 January 2011 are the data input into our inversion for mass change as a function of location in the western U.S.

Of the 1,576 GPS sites, we identify 1,276 recording primarily solid Earth's elastic response to mass change. We omit the 300 GPS sites that do not, consisting of 159 sites responding porously to groundwater changes, 57 sites responding to volcanic activity, and 84 sites influenced by interseismic strain accumulation at Cascadia subduction zone (McCaffrey et al., 2013), by the 2010 *M* 7.2 Baja earthquake (Rollins et al., 2015), or by other local interfering phenomena (Figure S4).

3.2. Omitting GPS Sites Responding Porously to Groundwater Change

We identify and omit the 10% of GPS sites reflecting primarily solid Earth's porous response to groundwater changes (Figure S4). As we describe in section 1, Earth's porous response to groundwater change is opposite that of Earth's elastic response to changes in the mass of snow and water. We identify and omit the 159 GPS sites recording primarily Earth's porous response to groundwater change on the basis of one or more of four criteria:

1. A site has a seasonal oscillation of more than 3 mm with a maximum height around April (at the time of maximum groundwater)

2. The site is subsiding faster than 2.5 mm/yr (in response to long-term groundwater pumping).
3. The site has strong episodic transients (due to groundwater pumping).
4. The site is located within 10 km of a groundwater pumping well.

We assess whether sites are responding porously by constructing maps with vector representations of the seasonal oscillations (as in Argus, Fu, et al., 2014, Figure S1). For each GPS site, we plot a vector. The length of the vector represents the peak-to-peak amplitude of the seasonal oscillation; the azimuth of the vector depicts the time of year of maximum vertical height, with 1 January being north, 1 April being east, 1 July being south, and 1 October being west. Such maps allow regional patterns in the timing of seasonal oscillations to be identified. We also construct maps comparing the locations of GPS sites and 20,000 groundwater pumping wells (obtained from California's Department of Water Resources and the Los Angeles Metropolitan Department of Water and Power).

Sixty-five percent of the 159 GPS sites responding porously are in six known large aquifers: 31 sites are in the San Joaquin Valley, 18 sites are in the Sacramento Valley, 26 sites are in sedimentary basins in metropolitan Los Angeles, 12 sites are in groundwater basins in and near Phoenix (Arizona), 10 sites are in groundwater basins in western Utah, and 5 sites are in the Napa and Sonoma Valleys north of San Francisco or in the Santa Clara Valley south of San Francisco (Chaussard et al., 2017; Forster, 2012; Knudsen et al., 2014; Miller & Shirzaei, 2015) (Figures 4 and S4). The remaining 35% of GPS sites with a groundwater signature are not associated with any large aquifer.

3.3. Omitting GPS Sites Affected by Volcanic Activity

We identify and omit the 4% of GPS sites affected by volcanic activity (Figure S4). Of the 57 GPS sites that we omit, 30 are located within 32 km of Long Valley Caldera (California) and are predicted by a Mogi model (Montgomery-Brown et al., 2015) to have risen faster than 0.25 mm/yr in response to renewed inflation of the magma chamber from late 2011 to 2014. We omit 7 GPS sites influenced by volcanic activity at Lassen Peak (California), 12 sites near Yellowstone hotspot (Wyoming), 5 sites at Mount Saint Helens (Washington), 2 sites at Three Sisters (Oregon), and 1 site near Medicine Lake (California). Uplift or subsidence centered on many of these volcanoes is observed with InSAR (Chang et al., 2010; Dzurisin et al., 2006; Parker et al., 2016; Wicks et al., 2006).

3.4. Removing Elastic Vertical Displacement Produced by Changes in Atmosphere Mass

We remove elastic vertical displacements produced by changes in atmospheric mass using the ERA-Interim reanalysis of the European Centre for Medium-Range Weather Forecasts (ECMWF) (Dee et al., 2011). We first divide the mean monthly surface pressure in ERA-Interim (at 3/4° intervals of latitude and longitude) by 9.81 m/s^2 to obtain atmospheric mass. We next calculate solid Earth's elastic response using the Green's functions for a gravitating, spherical, stratified Earth assuming PREM (Wang et al., 2012).

Changes in atmospheric mass associated with high-pressure and low-pressure weather systems lasting a few days typically produce vertical displacements of several millimeters. However, elastic vertical displacements produced by changes in atmospheric mass average away over a month to less than 3 mm. In the western U.S., monthly changes in atmospheric load amount to a maximum of 0.1 m in equivalent water thickness near the Pacific Ocean coast.

3.5. Removing Elastic Vertical Displacement Produced by Changes in Surface Water in Artificial Reservoirs

We next remove (from the GPS series) elastic vertical displacements produced by changes in surface water in artificial reservoirs recorded by the California Data Exchange Center (CDEC, 2017b). If such elastic displacements were not removed, the GPS sites adjacent to the artificial reservoirs could strongly bias the inversion for mass change. Using a forward model, we determine the vertical displacements generated by changes in surface water in artificial reservoirs measured by California Data Exchange Center using the Green's function (for PREM, Wang et al., 2012) specifying solid Earth's elastic response to a surface mass load. At each of the 22 largest reservoirs, we first identify all pixels at 1/256° intervals of latitude and longitude that are inside the shorelines of the reservoir (using the National Hydrography Dataset, 2017), next distribute changes in surface water recorded by CDEC evenly across the pixels in the reservoir, and then calculate (and remove) solid Earth's elastic response using the Green's functions for a gravitating, spherical, stratified Earth assuming

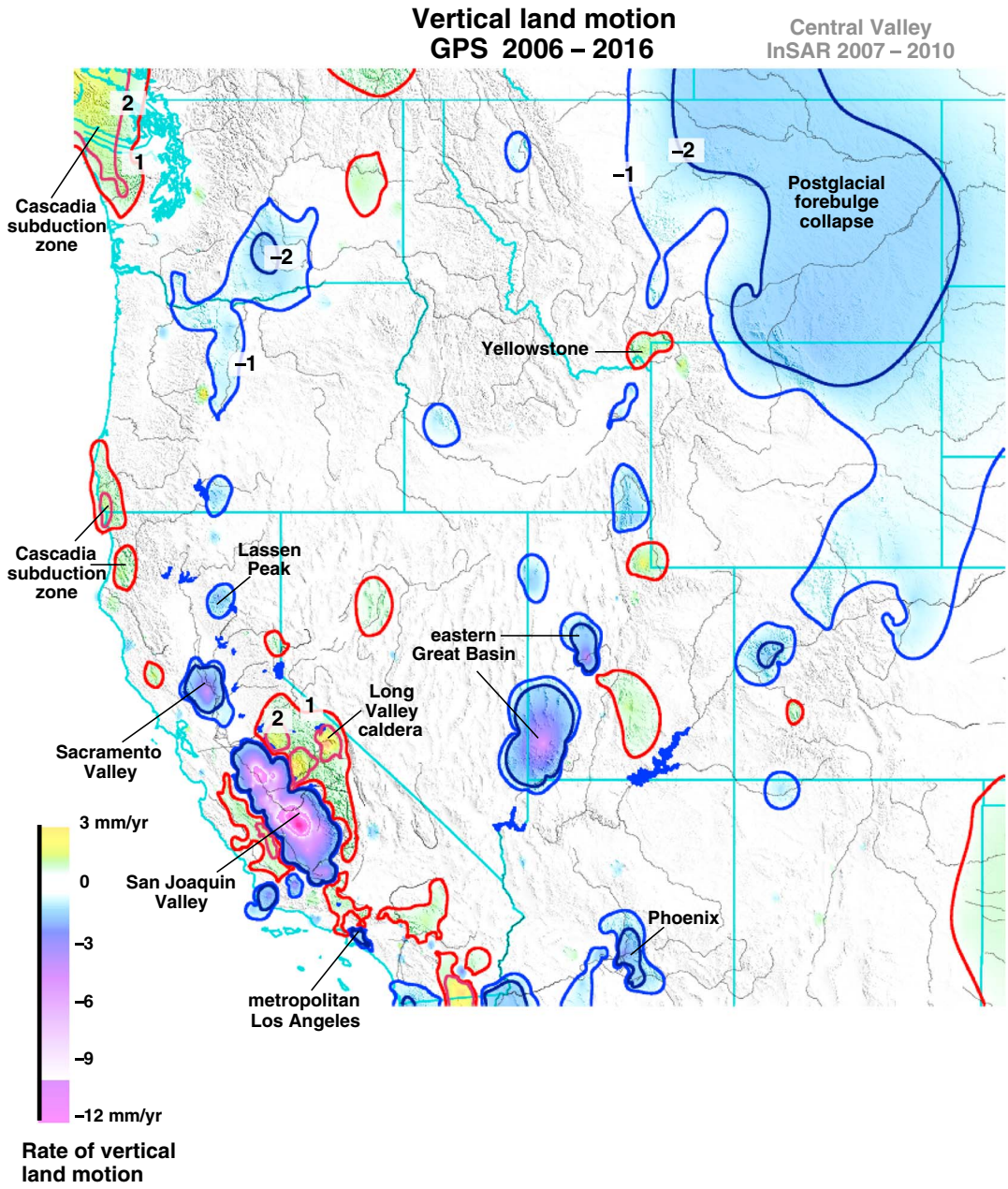

Figure 4. Mean rate of vertical motion from 2006 to 2016 determined by fitting a surface to the 1576 GPS sites in Figure S4 and to InSAR data from 2007 to 2010 in San Joaquin (Farr & Liu, 2014). Contours are at −2 mm/yr, −1 mm/yr, 1 mm/yr, and 2 mm/yr. Groundwater pumping has caused most of the San Joaquin Valley to subside at 10–250 mm/yr and parts of the Sacramento Valley, eastern Great Basin, and Phoenix to subside faster than 3 mm/yr. Volcanic activity produces vertical motion at Lassen Peak, Long Valley Caldera, and Yellowstone. Slow uplift of parts of the Washington, Oregon, and California coast reflects interseismic strain accumulation due to locking of the main thrust at Cascadia subduction zone. The surface is fit to the data using the GMT algorithm "surface" (Wesell & Smith, 1998).

PREM (Wang et al., 2012) (each pixel is a disk with a radius of about 0.22 km) (Figures S5 and S6). The 22 artificial reservoirs that we remove account for 95% of the surface water change in the southwestern U.S. At every GPS site, we have removed any elastic displacement greater than 3 mm produced by changes in surface water in artificial reservoirs.

Changes in surface water levels in Lake Shasta and Oroville Lake are 10 m to 30 m, many times greater than the change in the equivalent water thickness of snow and soil moisture in the adjacent mountain ranges

(of about 1 m). During drought from October 2011 to October 2015, the water level of Lake Oroville declined 35 m, causing GPS site ORVB to rise 10 mm, and the water level of Shasta Lake declined 19 m, causing GPS site P349 to rise 9 mm (Wahr et al., 2013) (Figure S7). If the elastic displacements of these sites were not corrected for, the values of change in snow and soil moisture would be incorrectly inferred.

At Shasta Lake and Lake Oroville, seasonal oscillations in surface water of a few cubic kilometers create vertical oscillations of several mm (Figure S7). At Lake Mead (Arizona, Nevada) and Lake Powell (Utah), sustained changes in surface water of several cubic kilometers produce sustained vertical displacements of several mm at GPS sites P006 and NVLM. Water volume changes at Lake Mead and Lake Powell are greater than those at Shasta Lake and Lake Oroville but are distributed across a greater area, so that the vertical displacements at GPS sites adjacent to Lake Mead and Lake Powell are comparable in size to the vertical oscillations at Shasta Lake and Lake Oroville.

Removing the elastic displacements produced by surface water changes at Lake Mead and Lake Powell leaves minor residuals (less than about 10 mm) at adjacent GPS sites, reflecting the small change in total water occurring in the Basin and Range desert (Figure S7). In contrast, removing the elastic vertical displacements produced by surface water changes at Shasta Lake and Lake Oroville leaves substantial residuals (greater than 10 mm), reflecting changes in snow, soil moisture, and possibly groundwater in the adjacent mountain ranges.

3.6. Removing Viscous Vertical Displacements Produced by Postglacial Rebound

We then remove (from the GPS series) vertical displacements associated with solid Earth's viscous response to unloading of the ice sheets 15 to 5 ka. We remove the predictions of present-day vertical motion from postglacial rebound model ICE-6G_C (VM5a), which is fit to nearly all available geologic relative sea level histories, geologic ice height change data, and geodetic rates of vertical land motion (Argus, Peltier, et al., 2014; Peltier et al., 2015). The forebulge of the former Laurentide Ice Sheet, which encompasses the United States, is now collapsing slowly. The model predicts subsidence of 0.5–1 mm/yr in the southwestern U.S. and of 1–2 mm/yr in the northwestern U.S. Removing the postglacial rebound model effectively reduces uplift in eastern Montana from 2 mm/yr to nearly zero but increases uplift in much of the western U.S. from nearly 0 to about 1 mm/yr (compare Figures S8–S10). We believe this residual uplift to be unrealistic and maintain it to result from inaccuracy in the estimate of the velocity of Earth's center defining the reference frame that vertical motions are estimated relative to (Argus, 2007; Dong et al., 2014; Riddell et al., 2017). We therefore next (in section 3.7) transform the vertical reference frame. A second hypothesis is that the viscosity of the North American Cordillera could be lower than assumed in the postglacial rebound model, resulting in a shorter characteristic time specifying the collapse of the forebulge and hence slower current vertical motions generated by postglacial rebound.

3.7. Transforming the Reference Frame of the Vertical Displacements

The velocity of the center of mass (CM) of Earth (consisting of the solid Earth, the ice sheets, continental water, the oceans, and the atmosphere) is the standard reference frame vertical motions are estimated relative to. The translational velocity of International Terrestrial Reference Frame 2008 (ITRF2008) (Altamimi et al., 2011) is defined by the velocity of CM as estimated by satellite laser ranging between LAGEOS and laser stations on Earth's surface. This estimate of the velocity of CM is, however, uncertain. The velocity of CM is specified along three perpendicular directions: X is parallel to the geocentric vector to 0°N 0°E, Y to 0°N 90°E, and Z to 90°N. Using spectral analysis and data decimation, Argus (2012) estimates the uncertainty to be just ±0.4 mm/yr in the X and Y directions but ±0.9 mm/yr in the Z direction (95% confidence limits). Dong et al. (2014) and Riddell et al. (2017) also find the Z component of the velocity of CM to be quite uncertain.

Argus (2007, 2012) proposes an alternative means of estimating the velocity of Earth's center: minimize the square of differences between geodetic measurements of vertical rates of land motion and their predictions from a postglacial rebound model. By implementing this method for global geodetic data and ICE-6G_C (VM5a), Argus, Peltier, et al. (2014, Figure S4) estimate the velocity of Earth's center relative to ITRF2008 to be X 0.18 mm/yr, Y −0.13 mm/yr, and Z 0.56 mm/yr. We transform all GPS site velocities by this translational velocity: in the western U.S., uplift is reduced by a uniform 0.37 mm/yr (compare Figures S10 and S11), yielding vertical motions that are nearer zero. Applying this translational velocity furthermore reduces differences between geodetic vertical motions observed in the central and eastern U.S. and those predicted by ICE-6G_C

(VM5a). Applying this translational velocity furthermore increases geodetic subsidence rates in the central and eastern U.S., resulting in a better alignment of the geodetic observations with forebulge subsidence at 2 mm/yr there in ICE-6G_C (VM5a).

3.8. Comparing Against Changes in Snow and Soil Moisture in Hydrology Models

We compare changes in total water storage inferred from GPS to two hydrology models. NLDAS-Noah, the North American Global Land Assimilation System (Mitchell et al., 2004), consists of values of snow water equivalent and of soil moisture each month at 1/8° intervals of latitude and longitude. We also compare to a composite hydrology model consisting of soil moisture in NLDAS-Noah and snow water equivalent in the Snow Data Assimilation System (SNODAS) (National Operational Hydrologic Remote Sensing Center, 2004; National Snow and Ice Data Center, 2017). Snow Telemetry (SNOTEL) measurements demonstrate snow water equivalent to be about 4 times thicker than in NLDAS-Noah (Pan et al., 2003). Our composite hydrology model incorporates SNODAS, which is fit to the SNOTEL data.

3.9. Comparing Against Changes in Total Water Inferred From GRACE

We also compare changes in total water storage inferred from GPS to those inferred from GRACE gravity in JPL's mass concentration solution (Watkins et al., 2015; Wiese et al., 2017). This "mascon" solution (see also Luthcke et al., 2013; Save et al., 2016) is less subject to leakage of the gravity signal outside a specific region than the traditional spherical harmonic solution. In JPL's mascon solution, changes in 3° spherical caps are determined directly from the satellite-to-satellite range-rate data. A regularization constraint is applied in space and time to reduce correlated errors (i.e., the anomalous north-south striping). The 3° spherical caps are 330 km in diameter, representing GRACE's native spatial resolution.

Wiese et al. (2016) next apply independent geophysical information to redistribute the mass change in each 3° mascon, thus inferring mass change at 1/2° intervals of latitude and longitude. First, a Coastal Resolution Improvement filter is applied to distinguish between mass changes on land and in the ocean. Second, gain factors are applied to correct the GRACE estimates of mass change for leakage of the gravity signal outside of narrow belts of water change. The gain factors are calculated on the basis of seasonal water oscillations in the hydrologic Community Land Model (Lawrence et al., 2011). Applying the gain factors increases mass change inside narrow belts of seasonal water change (such as the Sacramento-San Joaquin River basin) and decreases mass changes outside the belts. The resulting GRACE determination has a spatial distribution of mass change that becomes closer to the spatial distribution in the hydrology model. Applying the gain factors simply redistributes mass change within each 3° mascon; the total mass change in each mascon is unchanged.

4. Inversion

4.1. Solid Earth's Elastic Response to a Mass Load

Solid Earth's elastic response to a point load is specified by

$$u = m \times G(\Theta), \tag{1}$$

where u is the vertical displacement of Earth's surface (in m) at an angular distance Θ (in degrees) from the point load, m is the mass of the point load (in kg), and G is the Green's function (in m/kg), which depends on Θ. We use the Green's function for a gravitating, spherical, stratified Earth for PREM (Wang et al., 2012).

We numerically integrate the Green's functions to obtain a modified (Green's) function specifying solid Earth's elastic response to a disk with a specific radius. We calculate many such modified (Green's) functions, varying the disk radius so that the disk area is equal to the area of a rectangular spherical cap (pixel) between specific intervals of latitude and longitude. For example, in the inversion for mass load at 1/4° intervals of latitude and longitude, we calculate a modified (Green's) function for a disk with a radius of 13.91 km for the pixels at 38.125°N; the radii of the disks range from 14.43 km for the pixels at 32.125°N to 12.59 km for the pixels at 49.875°N. When we calculate the vertical displacements produced by changes in a hydrology model at 1/8° intervals of latitude and longitude, the radii of the disks are about 7 km. When we calculate the vertical displacement produced by changes in surface water in artificial reservoirs at 1/256° intervals of latitude and longitude, the disk radii are about 0.22 km.

We are calculating solid Earth's elastic response in a manner consistent with that in GRACE gravity analyses. In GRACE, scientists infer the change in the total mass of ice, snow, and water at Earth's surface after accounting for solid Earth's elastic uplift or subsidence in response to the surface load. In GRACE, this elastic response is calculated using spherical harmonic expansion, Legendre polynomials, and load Love numbers (Wahr et al., 1998, equation (7)). In this study, we calculate solid Earth's elastic response by integrating the Green's function (Wang et al., 2012). Solid Earth's elastic response is consistent between the two different formulations: solid Earth's elastic response is calculated for a gravitating, spherical, stratified Earth. As we describe in section 6, calculating solid Earth's elastic response for a nongravitating half-space yields vertical displacements that are overstated by a factor of 2.5. For a disk with a water thickness of 1 m and a radius of 20 km, we determine solid Earth's elastic response to be identical to that calculated by Wahr et al. (2013, Figure 1). We benchmarked the Green's function for a gravitating, spherical, stratified Earth for PREM (Wang et al., 2012).

The scientific literature emphasizes that solid Earth's elastic response depends on Earth's rheologic structure. But in truth solid Earth's elastic response to change in a mass load several tens of kilometers across is not very sensitive to Earth's structure. For a disk with a radius of 14 km, solid Earth's elastic response is similar for the PREM and Gutenberg Bullen A Earth structures (the difference at the load center is 7.5%, but the difference between the two Earth compositions decreases to less than 5% for loads several tens of kilometers across). For a 450 km × 60 km load (approximating the Central Valley), a stratified sphere with a sedimentary basin in the top 5 km predicts (as in the deepest part of Los Angeles Basin) elastic vertical displacement to be just 15% greater than a model with crystalline basement in the top 5 km.

4.2. Inversion of Vertical Displacements for Mass Change

To invert the GPS vertical displacement for changes in mass load as a function of location, we minimize

$$(\,(\mathbf{Ax}–\mathbf{b})/\sigma_1)^2 + \left(\nabla^2(\mathbf{x})/\sigma_2\right)^2, \tag{2}$$

where **A** is the design matrix of modified (Green's) functions specifying solid Earth's vertical displacement in elastic response to a surface mass load, **x** is a vector of the surface mass at all locations on the grid, **b** is a vector of the GPS observations of vertical displacement, ∇^2 is the Laplacian operator, σ_1 is the standard error in the GPS vertical displacement, and σ_2 is the standard error in the Laplacian constraint. We evaluate the Laplacian operator using a finite-difference approximation; that is, the right-hand term for a single mass element is $((x - (a + b + c + d)/4)/\sigma_2)^2$, where x is the value of water change in a mass element and a, b, c, and d are the values of mass change in the elements to the east, south, west, and north. Thus, the Laplacian operator is a smoothing constraint that limits water change in adjacent mass elements. Our inversion method is identical to that of Argus, Fu, et al. (2014) and Fu et al. (2015). The ratio of σ_1 to σ_2 defines the smoothing factor β in the prior two studies. We estimate change in mass elements at 1/4° intervals of latitude and longitude in the western U.S. (from 32°N to 49°N and from 125°W and 103°W). We set water change at mass elements in the ocean to zero.

We invert the monthly GPS vertical displacements in two ways. First, we invert for change in total water storage each month from January 2006 to the present relative to 1 January 2011 using the monthly GPS position-time series. Second, we invert for water change over a specific period of time using vertical displacements of GPS sites with observations at the beginning and at the end of the time period. The latter method allows changes in water storage during specific time periods and their uncertainties to be determined accurately (Figures 5–8). The former method allows the evolution of water storage in physiographic provinces to be evaluated (Figures 9 and 10).

4.3. Constraining Groundwater Change in Central Valley to an A Priori Model

In the preferred ("constrained") model in this study, we perform the inversion while constraining water change in Central Valley to an a priori model constructed on the basis of the Central Valley Hydrologic Model (CVHM) (Faunt, 2009; Faunt et al., 2015) from 2006 to 2013 and to the water-balance model of Xiao et al. (2017) from 2013 to 2016 (Figure 1b). This a priori model that we adapt for the inversion differs somewhat from that described in section 1 (in Figure 2b) in that we added a layer of groundwater loss distributed evenly across the Central Valley. In this a priori model assumed in the inversion, 25% of groundwater change occurs in Sacramento Valley (as opposed to the 2% in the model in the Introduction) and 75% of groundwater

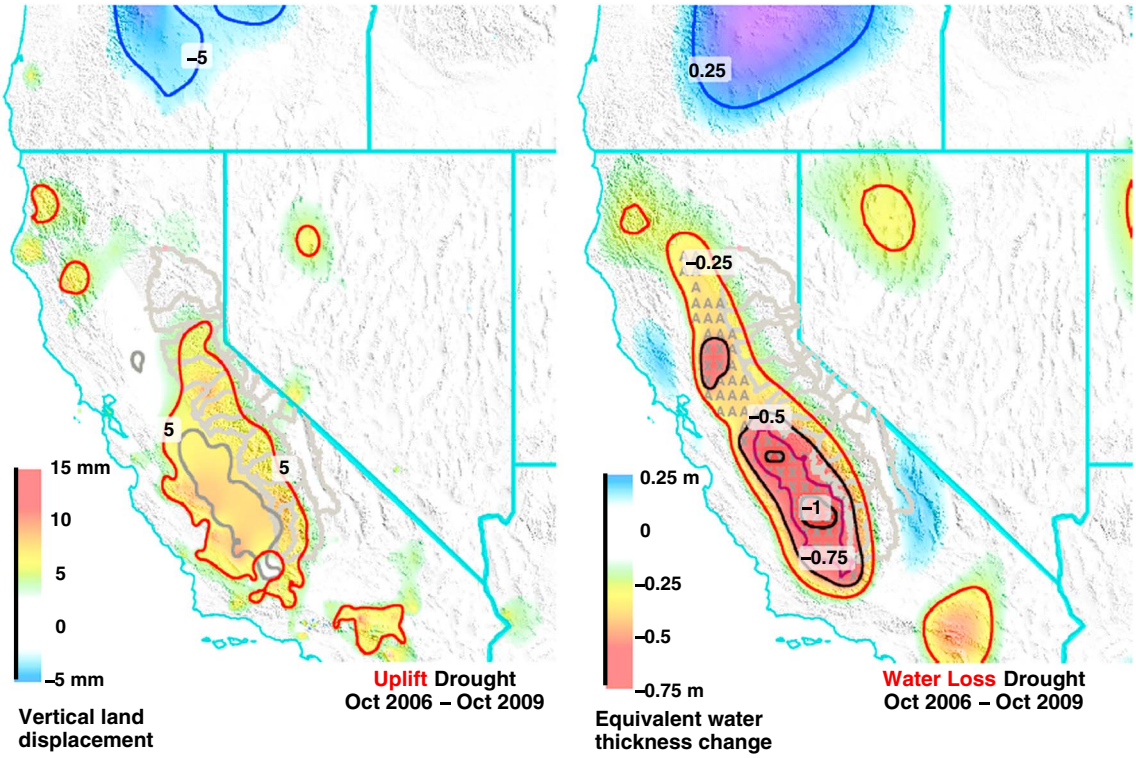

Figure 5. (left) Vertical land displacement from GPS and (right) change in total water storage during drought from October 2006 to October 2009. GPS data in the Central Valley are omitted in calculating the vertical land displacement. Total groundwater loss in Central Valley is set equal to −33 km^3 in the inversion: Groundwater loss at 1/4° pixels in the Central Valley (small gray letters) is set equal to −1.53 m (Zs), −1.15 m (Ys), −0.77 m (Xs), or −0.38 m (As).

change occurs in San Joaquin Valley. In this a priori model groundwater change is 4 times as large at the center of Tulare Basin as in the Sacramento Valley (Figures 5–8). During drought from October 2011 to October 2015, groundwater loss ranges from −1.64 m at the center of Tulare Basin (Zs in Figure 7) to −0.41 m in the Sacramento Valley (As).

In an alternate "unconstrained" model, we first remove elastic vertical displacement produced by the a priori model of groundwater change in section 1 (in Figure 2b), then invert for change in total water in all places including in the San Joaquin Valley, where no GPS sites record solid Earth's elastic response (Figure S12). Because solid Earth's elastic response is narrow in space, the estimates of water change in the mountain ranges adjacent to the Central Valley differ only slightly between the constrained model and the unconstrained model. For example, water loss in the Sierra Nevada during drought from October 2011 to October 2015 is just 4 km^3 less in the unconstrained model than in the constrained model. However, water loss in the Central Valley from October 2011 to October 2015 is twice as large in the unconstrained model (76 km^3, after adding back in the 34 km^3 implicitly removed from the GPS vertical displacements) as in the constrained model (34 km^3). We maintain that the constrained model determined on the basis of water-balance models of groundwater change is nearer truth than the unconstrained model, which has no constraints in the San Joaquin Valley. Setting Central Valley groundwater change equal to an a priori model in the inversion is essential for the comparison between GPS and GRACE of water change in the Sacramento-San Joaquin River basin.

4.4. Uncertainty in Water Change Inferred From GPS

We estimate uncertainties in changes in total water storage inferred from GPS using the dispersion of vertical displacements about the model fit to the data. The uncertainties that we estimate depend on the smoothing factor (ratio of σ_1 to σ_2 in equation (2), related to β in Fu et al., 2015) that we adopt, but not strongly so. Our uncertainties are dictated by this lateral Laplacian constraint and thus based on the consistency between vertical displacement estimates at nearby GPS sites.

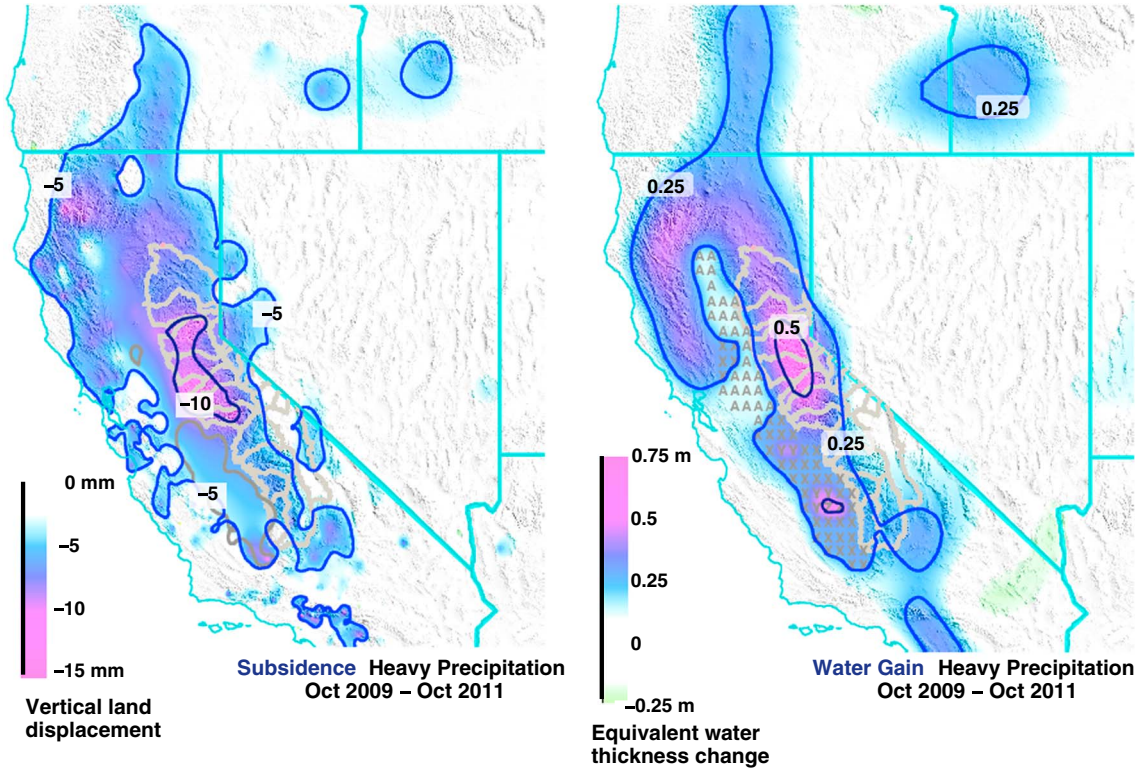

Figure 6. (left) Vertical land displacement from GPS and (right) change in total water storage during heavy precipitation from October 2009 to October 2011. GPS data in the Central Valley are omitted in calculating vertical land displacement. Total groundwater loss in Central Valley is set equal to +13 km^3 in the inversion: Groundwater loss at 1/4° pixels in the Central Valley (small gray letters) is set equal to 0.60 m (Zs), 0.45 m (Ys), 0.30 m (Xs), or 0.15 m (As).

We start by assigning each GPS vertical displacement a standard error of 1 mm and each Laplacian constraint between adjacent pixels a standard error of 18 mm. This 1 to 18 ratio results in a reasonable distribution of water thickness as a function of location (Figures S13 and S14, top). Using these beginning standard errors of 1 mm and 18 mm results in chi-square misfits that are significantly too large. The misfit in each inversion can be quantified by the normalized sample standard deviation (NSSD), which is defined to be the square root of reduced chi-square. We find the NSSD values to range from 1.4 to 4.6 depending on the month of the inversion (relative to 1 January 2011) or the time period of the inversion (e.g., October 2011 to October 2015). This simply means that the original assigned errors are too small by a factor of 1.4 to 4.6. We follow standard practice (e.g., Press et al., 1992) and multiply (scale upward) uncertainties in water change calculated using linear propagation of errors by the NSSD (thus assuming that the errors are random, not systematic) to obtain realistic uncertainties.

In the inversions for the monthly series from 2006 to 2017, we find the NSSD values to increase as the time from January 2011 lengthens. The NSSD is 2 mm for months within 2 years of January 2011, 2.5–3 mm for months 2 to 4 years from January 2011, and 3.5–4 mm for months 4 to 6 years from January 2011. The NSSDs in the inversions for specific time periods increase in similar fashion as the time period lengthens. The result indicates that the true uncertainty in vertical displacement is 2 mm for months 2 years apart and increases to 4 mm for months 5 years apart. This result is consistent with the conclusion that random walk is present in the GPS series (Amiri-Simkooei et al., 2017; Dmitrieva et al., 2015).

That the true uncertainty in a GPS vertical displacement is 2 to 4 mm is also indicated by the dispersion of GPS monthly displacements about a standard model. For the 1276 GPS position-time series, the root-mean-square misfit of a model consisting of an offset, a rate, and a sinusoid with a period of year has a median value of 3.3 mm, and quartile values of 2.7 and 3.5 mm. These RMS values overstate the true uncertainty because sustained fluctuations due to periods of drought or years of heavy precipitation are not included in the model.

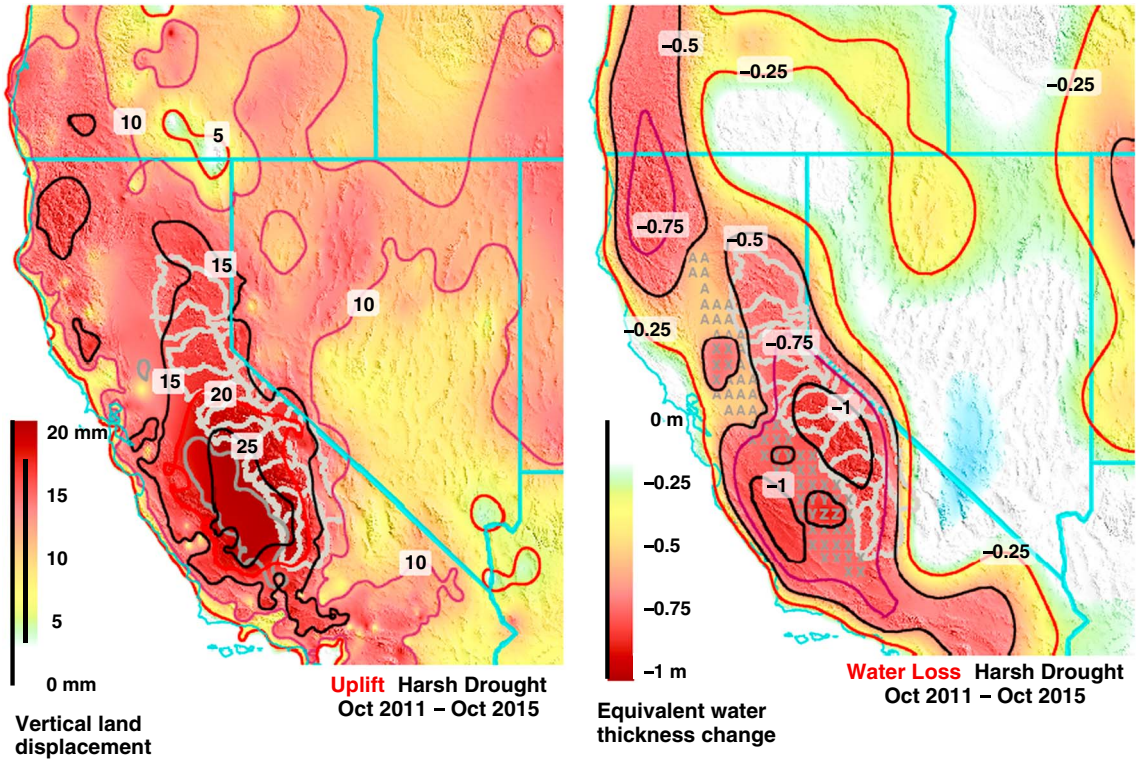

Figure 7. (left) Vertical land displacement from GPS and (right) change in total water storage during severe drought from October 2011 to October 2015. GPS data in the Central Valley are omitted in calculating the vertical land displacement. Total groundwater loss in Central Valley is set equal to −34 km^3 in the inversion: Groundwater loss at 1/4° pixels in the Central Valley (small gray letters) is set equal to −1.64 m (Zs), −1.23 m (Ys), −0.82 m (Xs), or −0.41 m (As).

In California, the 95% confidence limits in change in equivalent water thickness inferred from GPS range from 0.080 m for times 2 years apart to 0.150 m for times 5 years apart. GPS can accurately determine change in total water storage in each of the three mountain range provinces in California (the Sierra Nevada, Coast Ranges, and Klamath mountains, each with an area on the order of 50,000 km^2). The GRACE determination of total water storage is more tightly constrained than the GPS in areas 400 km in width and length (160,000 km^2 in area), such as the Sacramento-San Joaquin River basin.

4.5. Spatial Smoothing of the Water Change Estimates

The 1 to 18 ratio between the standard error in GPS vertical displacement and the standard error in the Laplacian constraint results in an optimal distribution of water thickness as a function of location (Figures S13 and S14, top). If we were to have taken the ratio to be 1 to 12, we would find smoothing to be too high from east to west across the Sierra Nevada (Figures S13 and S14 bottom left): inferred water change does not attain as high of a value as it should near the mountain crest, and too much water change is pushed out into the Great Basin. If we were to have taken the ratio to be 1 to 27, we would find too many local maxima and minima to arise (e.g., in Oregon during drought from 2011 to 2015).

The values of water change inferred from GPS do not depend very strongly on the ratio between the standard errors (Figures S13 and S14). If we were to substitute strong smoothing (σ_2 12 mm), we would find water loss in the Sierra Nevada during drought from 2011 to 2015 to decrease by 3 km^3 (from 45 to 42 km^3), a 6% reduction; weak smoothing (σ_2 27 mm) would increase the water loss by 3 km^3 (from 45 to 48 km^3), a 6% increase. For the season of heavy precipitation from October 2016 to April 2017, changing to strong smoothing (σ_2 12 mm) reduces water gain in the Sierra Nevada by 6 km^3, a 13% decrease, whereas weak smoothing (σ_2 27 mm) increases water gain by 6 km^3, a 13% increase. The weaker smoothing (σ_2 27 mm) collapses more of the water change into the Sierra Nevada than does the optimal smoothing (σ_2 18 mm), representing an advantage in this regard because it reduced GPS leakage outside of narrow belts of water change such as the Sierra Nevada (the leakage is similar to that for GRACE but less pronounced).

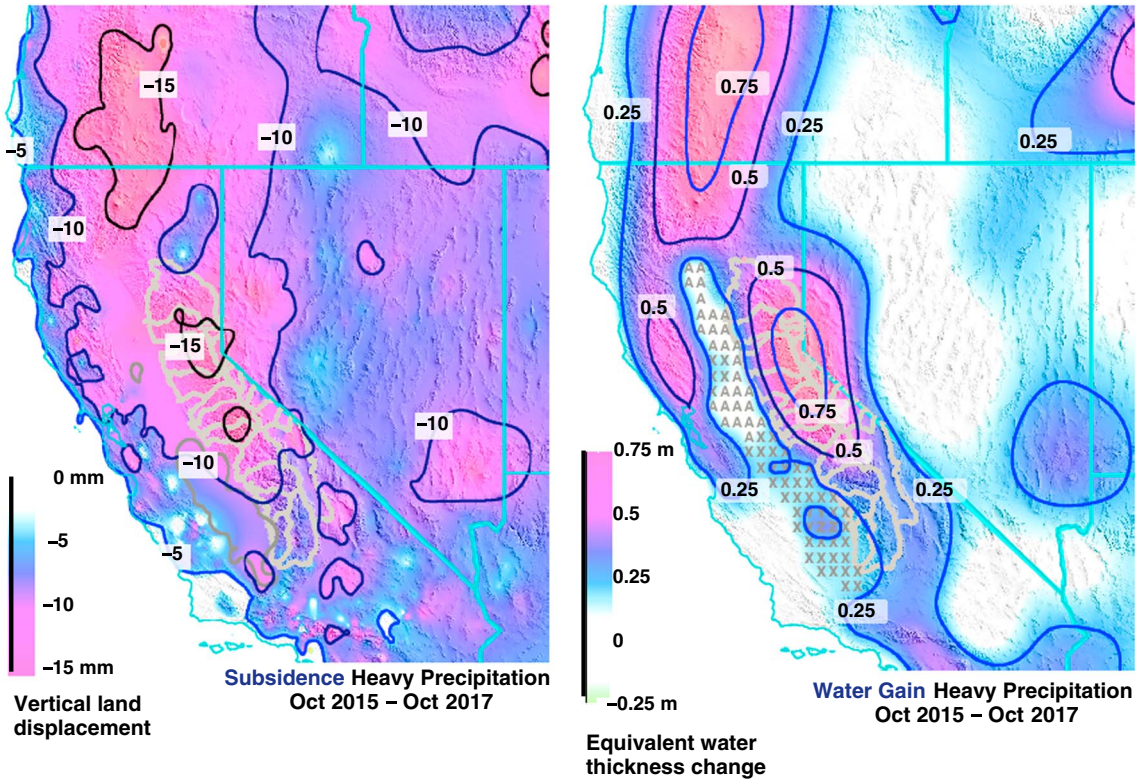

Figure 8. (left) Vertical land displacement from GPS and (right) change in total water storage during heavy precipitation from October 2015 to October 2017. GPS data in the Central Valley are omitted in calculating vertical land displacement. Total groundwater loss in Central Valley is set equal to +4 km^3 in the inversion: Groundwater loss at 1/4° pixels in the Central Valley (small gray letters) is set equal to 0.38 m (Zs), 0.29 m (Ys), 0.19 m (Xs), or 0.10 m (As).

The size of the uncertainties inferred from the dispersion in displacements about the model also does not depend strongly on the ratio between the standard errors (Figures S13 and S14). Substituting either strong smoothing (σ_2 12 mm) or weak smoothing (σ_2 27 mm) would change the RMS misfit by less than 10% for either the drought period from 2011 to 2015 (from 3.8 mm to 4.0 mm or to 3.7 mm) or the heavy precipitation season from October 2016 to April 2017 (from 2.6 mm to 2.7 mm or to 2.6 mm).

4.6. Inversion of Synthetic Vertical Displacements

To test GPS's capability to infer changes in total water storage, we perform an inversion of synthetic data generated from a hydrology model. We calculate vertical displacements at each of the GPS sites (each month a GPS site was observed from January 2006 to June 2015) produced by water changes in the composite hydrology model consisting of snow water equivalent in SNODAS and soil moisture in NLDAS-Noah. We next inverted the synthetic vertical displacements using the same methods as we do for the real GPS data. We find the increase in total water storage during heavy precipitation from October 2010 to April 2011 to be recovered fairly well, although the inferred water changes are smoothed relative to the tight belts of snow accumulation in the model (Figure S15). Thus, the inferred water change leaks outside of narrow areas of true water change, as for GRACE but much less so. We also find the evolution of total water storage in large areas such as the northern Rocky Mountains province and the Sacramento-San Joaquin River basin to be recovered very well, with the inferred water change nearly matching the model (Figure S16).

5. Results

5.1. Seasonal Changes in Total Water Storage Inferred From GPS

In this study, we extend the GPS characterization of seasonal water storage from California, Oregon, and Washington east into the eight Mountain States. Argus, Fu, et al. (2014) find the mean seasonal water oscillation in the Sierra Nevada and Klamath mountains (in California) to be 0.6 m in equivalent water thickness and to decrease sharply to 0.1 m going east into the dry Great Basin and west toward the Pacific coast. Water

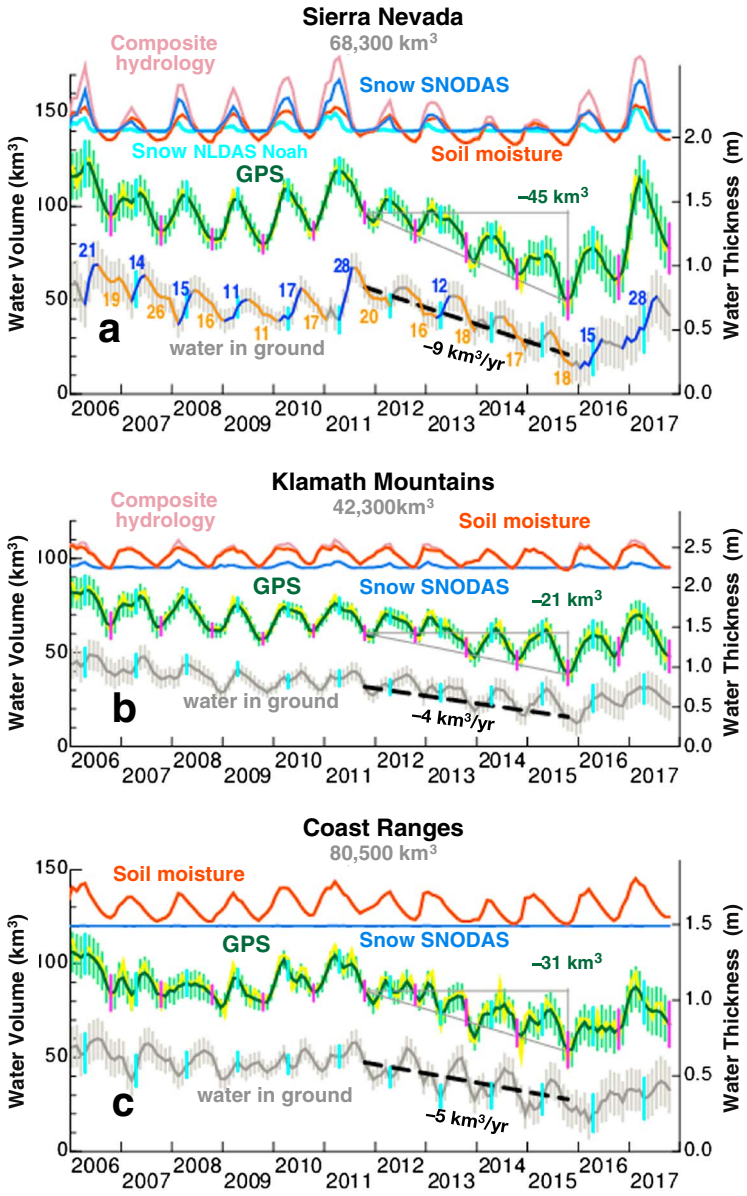

Figure 9. Changes in total water storage in the (a) Sierra Nevada, (b) Klamath mountains, and (c) Coast Ranges determined using GPS are compared to those in a composite hydrology model. The composite hydrology model (pink) consists of snow water equivalent in SNODAS (blue) and soil moisture in NLDAS-Noah (red). Changes in total water storage are observed with GPS (green) to be sustained over periods of drought and years of heavy precipitation; such sustained changes are not in the hydrology model. Error bars in the GPS data are 95% confidence limits. The Sierra Nevada, Klamath mountains, and Coast Ranges are observed with GPS to have lost 45, 21, and 31 km^3, respectively, during severe drought from October 2011 to October 2015. Change in groundwater (gray) is inferred to be total water change from GPS minus the sum of snow and soil moisture in the hydrology model. Changes in groundwater are also inferred to be sustained over periods of drought and years of heavy precipitation. The Sierra Nevada, Klamath mountains, and Coast Ranges are inferred to have lost groundwater at 9, 4, and 5 km^3/yr, respectively, from October 2011 to October 2015 (black dashed lines). Melting snow seeps into the Sierra Nevada in the spring (blue segments of the groundwater curve, blue numerals specify water gain in cubic kilometers); Groundwater leaves the Sierra Nevada in the summer (orange segments of the groundwater curve, orange numerals specify water loss in cubic kilometers). The magenta vertical bars on the GPS series mark the month of October. The light blue bars on the groundwater series mark the month of April. See Figure 1 for the location of the three physiographic provinces.

storage is maximum in April when snow accumulation is greatest and minimum in October when snow accumulation is insignificant. Fu et al. (2015) find the mean seasonal water oscillations in the Cascade Ranges (in Oregon and Washington) to be 0.5 m and to decrease sharply to 0.1 m going east into the dry

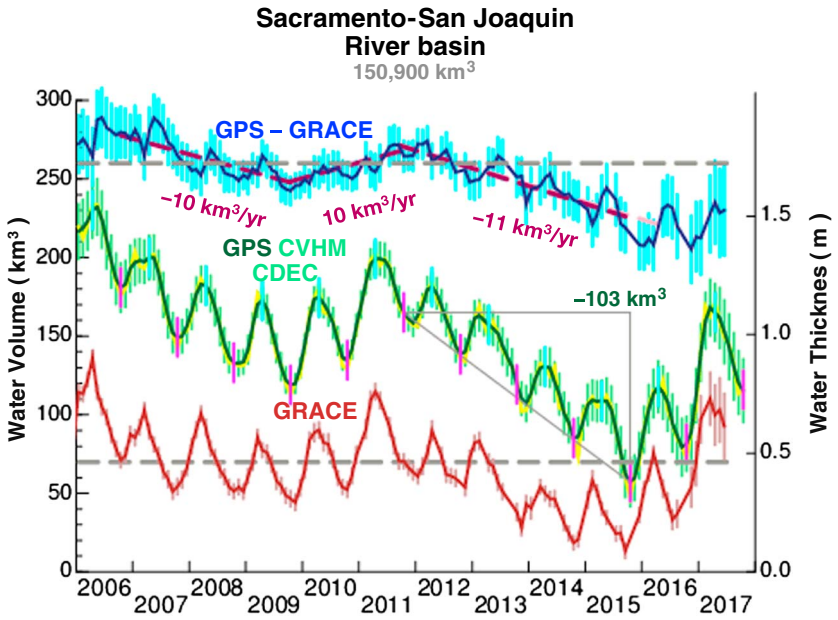

Figure 10. Change in total water storage in the Sacramento-San Joaquin River basin inferred from GPS/CVHM/CDEC (green) and estimated from GRACE (brown). The GPS/CVHM/CDEC determination consists of water change in the Sierra Nevada and adjacent mountains inferred from GPS, groundwater change in the Central Valley Hydrologic Model (CVHM) (Faunt et al., 2015), and surface water change in artificial reservoirs measured by the California Data Exchange Center (California Data Exchange Center, 2017b). Error bars in the GPS series are 95% confidence limits. The magenta vertical bars on the GPS series mark the month of October. The light blue vertical bars on the GPS series mark the month of April. See Figure 1 for the location of the Sacramento-San Joaquin River basin.

Columbia Plateau. Herein, we find the mean seasonal oscillation to be at most 0.6 m in the Northern Rocky Mountains, 0.4 m in the Middle Rocky Mountains, and 0.3 m in the Southern Rocky Mountains (Figure S17). We find the mean seasonal oscillation to be less than 0.2 m in the Colorado Plateau and less than 0.1 m in the Basin and Range. Furthermore, the mean increase in equivalent water thickness from October to April inferred from GPS is similar to that in the composite hydrology model. Although the seasonal water oscillations inferred from GPS are smeared in space relative to the tight clustering of snow and soil moisture in the mountain ranges in the hydrology model, the total seasonal water oscillation inferred from GPS over the broader belt is nearly equal to that in the model. The strong resemblance in seasonal water oscillations between the model and that inferred with GPS brings confidence that GPS is capable of accurately determining changes in total water storage.

Argus, Fu, et al. (2014) and Fu et al. (2015) find that in the Sierra Nevada, Klamath Mountains, and Cascade Ranges, the seasonal oscillations in total water storage inferred from GPS are nearly equal to those in the composite hydrology model consisting of snow in SNODAS and soil moisture in NLDAS-Noah. But the two studies find seasonal water oscillations inferred from GPS exceed those in the pure NLDAS-Noah hydrology model of snow and soil moisture. This finding supports the conclusion of Pan et al. (2003) that snow in NLDAS-Noah is too small by a factor of 2 to 4. The changes in total water storage inferred from GPS that we infer in this study confirm the characterization from the two prior studies. The finding that the composite hydrology model is more accurate than the NLDAS-Noah hydrology model is critical because we later (in section 5.3) integrate the GPS determination of water change and the composite hydrology model to infer changes in groundwater in the mountain ranges.

5.2. Sustained Changes in Total Water Storage During Periods of Drought or Heavy Precipitation Inferred From GPS

We next quantify changes in total water storage inferred from GPS over periods of drought or heavy precipitation. In the western U.S., snow typically accumulates on the ground from October to around April then melts in the late spring and summer, leaving negligible snow around 1 October. Because snow accumulation in October is negligible, we quantify changes in total water storage inferred from GPS from October to

October. Soil moisture changes are also small in the long term in the hydrology models (in NLDAS-Noah less than 6 km^3 in the Sierra Nevada, less than 7 km^3 in the California Coast Ranges, and less than 5 km^3 in the Klamath mountains). As we described in section 3, the changes in total water storage that we infer from GPS exclude surface water changes in artificial reservoirs. The water changes from October to October inferred from GPS that we present next are therefore mainly changes in water in the ground.

During drought from October 2006 to October 2009, parts of California's mountain ranges rose 3 to 7 mm in elastic response to water loss (Figure 5). From the inversion of the GPS measurements of vertical displacement, we infer the Sierra Nevada to have lost 15 ± 19 km^3 of water, the Coast Ranges to have lost an insignificant 7 ± 17 km^3 of water and the Klamath mountains to have lost 7 ± 12 km^3 of water (Figure 9). The 15 km^3 water loss in the Sierra Nevada amounts to an average decrease in equivalent water thickness of 0.22 ± 0.28 m. The three mountain provinces (the Sierra Nevada, the California Coast Ranges, and the Klamath mountains) lost a total of 29 ± 28 km^3 of water, yielding a mean decrease in equivalent water thickness of 0.15 ± 0.15 m. The uncertainties following the "±" signs are realistic 95% confidence limits, not the usual 1σ errors. These inferred water changes from October 2006 to October 2009 are somewhat uncertain because the Plate Boundary Observatory of GPS sites was deployed between 2004 and 2008.

During heavy precipitation from October 2009 to October 2011, most of California's mountains subsided 5 to 12 mm in elastic response to water gain (Figure 6). From the GPS vertical displacements, we infer the Sierra Nevada to have gained a significant 18 ± 14 km^3 of water, the Coast Ranges to have gained 7 ± 13 km^3 of water, and the Klamath mountains to have gained an insignificant 3 ± 9 km^3 of water (95% confidence limits). The 18 km^3 water gain in the Sierra Nevada amounts to an average increase in equivalent water thickness of 0.26 ± 0.20 m. The three mountain provinces gained a total of 28 ± 21 km^3 of water, yielding a mean increase in equivalent water thickness of 0.15 ± 0.11 m.

During harsh drought from October 2011 to October 2015, California's mountain ranges rose 10 to 25 mm in elastic response to water loss (Figure 7). From the GPS vertical displacements, we infer the Sierra Nevada to have lost a significant 45 ± 21 km^3 of water, the Coast Ranges to have lost a significant 31 ± 20 km^3 of water, and the Klamath mountains to have lost a significant 21 ± 14 km^3 of water (Figure 9). The 45 km^3 water loss in the Sierra Nevada amounts to an average decrease in equivalent water thickness of 0.66 ± 0.31 m. The three mountain provinces lost a total of 97 ± 34 km^3 of water, yielding a mean increase in equivalent water thickness of 0.51 ± 0.18 m. This water loss of 97 km^3 during harsh drought from October 2011 to October 2015 is 1.5 times the water gain of 65 km^3 in the rainy season of the 6 months of heavy precipitation from October 2010 to April 2011.

During heavy precipitation from October 2015 to October 2017, California's mountains subsided 5 to 15 mm in elastic response to water gain (Figure 8). From the GPS vertical displacements, we infer the Sierra Nevada to have gained a significant 28 ± 18 km^3 of water, the Coast Ranges to have gained 14 ± 17 km^3 of water, and the Klamath mountains to have gained 9 ± 12 km^3 of water (95% confidence limits). The 28 km^3 water gain in the Sierra Nevada amounts to an average increase in equivalent water thickness of 0.41 ± 0.26 m. The three California mountain provinces gained a total of 51 ± 34 km^3 of water, yielding a mean increase in equivalent water thickness of 0.27 ± 0.18 m. This water gain of 51 km^3 during heavy precipitation from October 2015 to October 2017 is 50% of the water loss of 97 km^3 during harsh drought from October 2011 to October 2015.

In summary, we find there are large changes in total water storage during periods of drought or heavy precipitation. These changes cannot be snow because snow accumulation is insignificant in October. Such sustained water changes are absent in the hydrology models. For example, the 97 ± 34 km^3 of water inferred from GPS to be lost in the Sierra Nevada, the Coast Ranges, and Klamath mountain ranges from October 2011 to October 2015 far exceeds the 18 km^3 of snow and soil moisture lost in the composite hydrology model. Either changes in soil moisture are far understated in the hydrology models or there are changes in groundwater in river alluvium or in fractured crystalline basement in the mountain ranges that are not accounted for in the hydrology models.

5.3. Implications for Water Processes: Parching and Seeping

Integration of water changes inferred from the GPS and the composite hydrology model yields insight into water cycle processes. We next infer change in water in the ground to be change in total water inferred

from GPS minus the sum of snow in SNODAS and soil moisture in NLDAS-Noah (Figure 9, gray curve). Water in the ground could be either deep soil moisture not in the hydrology model or groundwater in river alluvium or in fractured crystalline basement.

The ground in the Sierra Nevada was parched of water in the summer and fall of each year from 2006 to 2015, reducing water in the ground by 11 to 26 km^3 each year (Figure 9, orange segments). Parching of water from the ground in the mountain ranges accumulated during harsh drought from October 2011 to October 2015. Groundwater (or deep soil moisture not in the hydrology model) is inferred to have been lost at a mean rate of 9 km^3/yr in the Sierra Nevada, at 5 km^3/yr in the Coast Ranges, and at 4 km^3/yr in the Klamath Mountains.

Melting snow seeped into the ground in the Sierra Nevada in the spring of years of heavy precipitation. In each of 2006, 2011, and 2017, the 3 years with the greatest snow accumulation, 21 to 28 km^3 of rain and melting snow is inferred to have seeped into the ground (Figure 9, blue segments). In 2011, a total of 28 km^3 of water infiltrated the ground. In 2017, 28 km^3 of water infiltrated the ground, replenishing water that was parched from the ground during the 4 years of harsh drought from October 2011 to October 2015.

Thus, the finding that substantial water changes are sustained over periods of drought or heavy precipitation implies the existence of water cycle processes (the parching of water from and the seeping of water into the ground) that are understated in the hydrology models. Although this inference depends on the accuracy of the composite hydrology model that we adopt, we nevertheless look forward to using our GPS determinations of changes in total water storage to constrain their water-balance models.

5.4. Change in Total Water Storage in the Sacramento-San Joaquin River Basin

Several studies have inferred change in total Central Valley groundwater from GRACE following the method of Famiglietti et al. (2011). Central Valley groundwater change is taken to be change in total water storage in the Sacramento-San Joaquin (SSj) River Valley inferred from GRACE minus the change in the sum of snow water equivalent, soil moisture, and artificial reservoir surface water in a hydrology model. The Central Valley is inferred to have lost about 20 km^3 of groundwater during drought from October 2006 to October 2009 and an additional 30 km^3 of groundwater during harsh drought from October 2011 to October 2015 (Famiglietti et al., 2011; Scanlon et al., 2012; Xiao et al., 2017). The Central Valley groundwater change series that we infer from GRACE (Figure 1b, pink dots) approximately matches that in the Central Valley Hydrologic Model (CVHM) from 2006 to 2013 (Faunt et al., 2015). During drought from October 2006 to October 2009, the Xiao et al. (2017) water-balance model has significantly less groundwater loss (16 km^3) than CVHM (32 km^3), suggesting that the two hydrology models may be uncertain.

However, the GRACE inference of groundwater change depends strongly on the hydrology model and, as we presented in section 5, water changes in the mountain ranges inferred from GPS over periods of drought are greater than in the hydrology model. For example, during harsh drought from October 2011 to October 2015, water loss in the mountain ranges in the SSj River basin is inferred from GPS to be 57 ± 30 km^3, far exceeding the 12 km^3 loss of soil moisture in the hydrology model. If we were to, in the GRACE calculation, remove the GPS determination of water change in the mountain ranges in the SSj River basin (as opposed to that in the hydrology model), we would find groundwater change in Central Valley to be about zero.

We next calculate change in total water storage in the SSj River basin to be the change in the sum of water in the mountain ranges inferred from GPS, surface water in artificial reservoirs from CDEC, and groundwater change in Central Valley in the CVHM/Xiao water-balance model. Water loss during drought from October 2006 to October 2009 is inferred to be 59 ± 28 km^3, water gain during heavy precipitation from October 2009 to October 2011 is inferred to be 43 ± 15 km^3, and water loss during severe drought from October 2011 to October 2015 is inferred to be 104 ± 30 km^3 (Figure 10, green curve). The 104 km^3 of water loss from October 2011 to October 2015 consists of 13 km^3 of surface water loss in artificial reservoirs from CDEC, 34 km^3 of groundwater loss in the Central Valley in the CVHM/Xiao model, and 57 km^3 of water loss in the mountain ranges inferred from GPS. We hereinafter refer to this GPS/CDEC/CVHM determination as being "inferred from GPS."

We are finding water changes in the SSj River basin inferred from GPS to differ somewhat from those inferred from GRACE. Although the overall pattern of water loss during drought and water gain during heavy

precipitation is similar between the two techniques, the estimates of water loss during drought and water gain during heavy precipitation are greater for GPS than for GRACE (Figure 10, blue curve). Water loss during drought from October 2006 to October 2009 inferred from GPS is a marginally significant 35 ± 32 km^3 greater than inferred from GRACE (95% confidence limits). Water gain during heavy precipitation from October 2009 to October 2011 inferred from GPS is 19 ± 21 km^3 greater than inferred from GRACE. Water loss during drought from October 2011 to October 2015 inferred from GPS (104 km^3) is a significant 47 ± 33 km^3 greater than inferred from GRACE (57 km^3). There are three possible explanations for this discrepancy.

First, slow tectonic uplift of the Sierra Nevada may reduce the discrepancy, but only slightly. If epeirogenic uplift of the Sierra Nevada were to occur at a steady 0.5 mm/yr, then 2 of the 24 mm of Sierra uplift observed during harsh drought from October 2011 to October 2015 would be of tectonic origin. Sierra Nevada water loss over the time period would be reduced by 8% (=2 mm/24 mm) from 45 km^3 to 41 km^3, lessening the discrepancy ever so slightly.

Second, the gain factor applied to account for leakage of the GRACE gravity signal (Landerer & Swenson, 2012) may be slightly underestimated. The gain factor is calculated by Wiese et al. (2016) from the spatial variations in seasonal water oscillations in the Community Land Model (Lawrence et al., 2011). Because the hydrology model does not include Central Valley groundwater changes, the gain factors inferred from the model may understate the true leakage. Moreover, the spatial distribution of the true long-term water changes may be clustered tighter in space than the seasonal water oscillations in the model. Indeed, we find that, for a larger SSj mask that is less subject to leakage error, the differences between the GPS and the GRACE determinations of water change are less significant (Figures S18 and S19).

Third, groundwater loss in the Central Valley from October 2011 to October 2015 may be significantly less than the 34 km^3 inferred from GRACE and the hydrology model. If groundwater loss in the Central Valley during the 4 years of harsh drought were 17 km^3 (as opposed to 34 km^3), then the difference between the GPS and the GRACE determinations of water loss in the SSj River basin would be a (marginally) significant 33 ± 33 km^3.

Water loss in the SSj River basin during harsh drought from October 2011 to October 2015 may truly be about 72 km^3, a value at the lower limit of the GPS determination (104 ± 30 km^3) and at the upper limit of the GRACE determination (57 ± 13 km^3). If this were true, the 72 km^3 of water loss in the SSj River basin could consist of the known 15 km^3 of surface water loss in artificial reservoirs, about 37 km^3 of water loss in the mountain ranges (near the lower limit of the GPS determination of 57 ± 30 km^3) and about 20 km^3 of groundwater loss in Central Valley.

5.5. Dependence of Water Changes Inferred From GPS on the A Priori Model of Central Valley Groundwater Change

The temporal evolution and spatial distribution of Central Valley groundwater change (in Figure 1b) is uncertain. However, our determination of water changes from GPS does not depend strongly on what we assume the a priori model of groundwater change to be. If we were to double groundwater change in the Central Valley, we would estimate water loss in the Sierra Nevada during drought from October 2011 to October 2015 to be just 3 km^3 smaller. If we were to halve groundwater change in the Central Valley, we would estimate water loss in the Sierra Nevada during the harsh drought to be just 2 km^3 larger.

But changing our a priori model of Central Valley groundwater change would change our determination of water change in the Sacramento-San Joaquin River basin. If we were to double groundwater change in the Central Valley, then water change in the SSj River basin from October 2011 to October 2015 would increase from 104 to 135 km^3 (because Central Valley groundwater change would increase from 34 to 68 km^3). If we were to halve groundwater change in the Central Valley, then water change in the SSj River basin during the harsh drought would decrease from 104 to 89 km^3 (because Central Valley groundwater change would decrease from 34 to 17 km^3).

Doubling Central Valley groundwater change would increase the difference between GPS and GRACE estimates of water change in the SSj River basin from October 2011 to October 2015, whereas halving Central Valley groundwater change would reduce the difference to a (marginally) significant 33 ± 33 km^3. Thus,

halving Central Valley groundwater loss during drought from October 2011 to October 2015 in the CVHM/Xiao model could reconcile the GPS and GRACE determinations.

5.6. Dependence of Water Changes Inferred From GPS on Assumptions About Postglacial Rebound and the Vertical Reference Frame

If we were to not transform the reference frame that the vertical displacements are estimated relative to, we would find the GPS estimate of water loss from October 2011 to October 2015 to be enlarged by 3 km^3 in the Sierra Nevada (from 45 to 42 km^3) and by 4 km^3 in the SSj River basin (from 104 to 100 km^3). If we were to neither remove postglacial rebound nor transform the vertical reference frame, we would find the GPS determination of water loss from October 2011 to October 2015 to be reduced by 3 km^3 in the Sierra Nevada (from 45 to 48 km^3) and by 4 km^3 in the SSj River basin (from 104 to 108 km^3).

6. Discussion

6.1. Comparison With Amos et al., 2014

Amos et al. (2014) maintain that from 2006 to 2014 the Sierra Nevada and Coast Ranges rose at 1 to 3 mm/yr in elastic response to groundwater loss in the Central Valley. In this study, we demonstrate that, if solid Earth's elastic response is properly determined, groundwater loss in the Central Valley at a mean rate of 4 km^3/yr from 2006 to 2016 produces elastic uplift of the Sierra Nevada and Coast Ranges at 0.6 mm/yr, accounting for 40% of the observed uplift of 1.5 mm/yr. We calculate solid Earth's elastic response to be 30% smaller than Amos et al. (2014).

We first replicate the model of Amos et al. (2014) using the formula in their article (from Jiang et al., 2010). This formula is based on the rock mechanic synthesis of Jaeger et al. (2007) and specifies solid Earth's elastic response to a surface load placed on top of a homogeneous half-space. An unnatural element of Amos et al.'s (2014) implementation of the formula is that they subtract a constant (K) from all values of vertical displacement and thus they find unrealistic subsidence of 1.0 mm/yr at a distance of 1,000 km from the load. On the basis of their formula and their Figure 2, we deduce the value of K must be −7.32 mm/yr. We verify that our calculation of their model (Figure 11, pink curve) is identical to their calculation (Amos et al., 2014, Figure 2 gray diamonds) by overlaying the two illustrations and adjusting the vertical and horizontal axes to match.

As we state in section 1, we next construct a model with a surface load identical to that in Amos et al. (2014) but calculate solid Earth's elastic response for a gravitating, stratified, sphere using the Green's function for PREM (Wang et al., 2012). In the model, groundwater loss at 4 km^3/yr is distributed evenly over a 450 km × 60 km rectangle, resulting in a decrease in equivalent water thickness of 0.148 m/yr over the rectangle. The model is nearly two dimensional in that the length of the zone is 8 times its width, but the model is not two dimensional because the surface load is approximated by a spherical cap and solid Earth's elastic response is calculated for a sphere. We find maximum uplift at the load center to be 1.15 mm/yr, 30% less than the 1.65 mm/yr in Amos et al. (2014). Moreover, we find uplift to decline to zero at distances very far from the load. We construct this nearly two-dimensional model to compare solid Earth's elastic response between us and Amos et al. (2014). In section 5, we adapt a three-dimensional model that more realistically specifies the distribution of groundwater change in the Central Valley. In the three-dimensional model, nearly all groundwater change occurs in the San Joaquin Valley; the 450 km × 60 km rectangle in the two-dimensional model well approximates the length and width of San Joaquin Valley.

What is the cause of the significant difference between solid Earth's elastic response in this study and that in Amos et al. (2014)? We constructed a series of intermediate models to answer this question. We find the following explanation. First, the homogeneous half-space model of D'Urso and Marmo (2013) is nearly equal to that of Amos et al. (2014), except for the unnatural translation introduced by Amos et al. (2014). We maintain this translation to be unjustified and that there should not be subsidence in the far field. The elastic response calculated from D'Urso and Marmo (2013), if translated downward by −0.45 mm/yr (top diagram in Figure S20, dotted orange curve), differs slightly from the elastic response of Amos et al. (2014) (pink curve). Second, the rheology assumed by Amos et al. (2014) is slightly stiffer than that in the top crustal layer of PREM. Therefore, vertical displacement in elastic response to a surface load is 30% greater for PREM than for the Amos et al. (2014) rheology (Figure S20, top diagram). Third, going from a nongravitating,

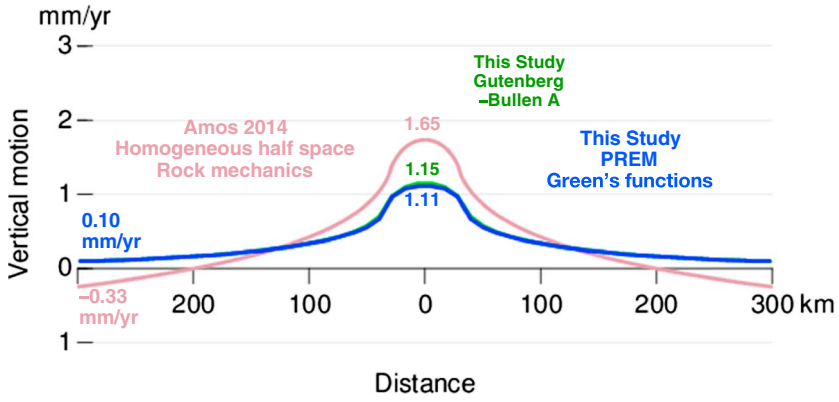

Figure 11. Two-dimensional models of elastic uplift produced by Central Valley groundwater loss. Solid Earth's elastic response to unloading of Central Valley groundwater water at -4 km^3/yr over a region 450 km long parallel to the axis of Central Valley and 60 km wide. Vertical motion calculated by Amos et al. (2014) using the rock mechanic formulation of Jaeger et al. (2007) for a homogeneous rheology on a flat Earth is compared to vertical motion calculated in this study assuming Green's functions for a layered Earth assuming the preliminary reference Earth model (Dziewonski & Anderson, 1981; Wang et al., 2012) and the Gutenberg-Bullen A Earth model (Farrell, 1972). Uplift at the center of Central Valley and at a distance of 300 km from the Central Valley is given. The gradient in vertical motion adjacent to the Central Valley is twice as steep in Amos et al. (2014) as in this study.

homogeneous half-space to a gravitating, homogeneous sphere reduces vertical displacement by a factor of 2.5 (Figure S20, middle diagram). Solid Earth's elastic response in the gravitating sphere is just 40% of that in the nongravitating half-space. This is the biggest difference between solid Earth's elastic response in this study and that in Amos et al. (2014). Fourth, going from a homogeneous, gravitating sphere to a stratified, gravitating sphere reduces the elastic response by 9% at the load center and by 27% at a distance of 50 km from the load (Figure S20, middle diagram). Fifth, substituting a sedimentary layer in the top 5 km into PREM increases the elastic response by just 14% (Figure S20, bottom diagram). Hence, solid Earth's elastic response to surface loads tens of kilometers across is not very sensitive to Earth's rheology.

6.2. Comparison With Borsa et al., 2014

Borsa et al. (2014) find land uplift at GPS sites across the western U.S. to have a median value of 4 mm in March 2014 relative to Earth's surface mean elevation from around 2006 to 2012. They attribute this uplift to solid Earth's elastic response to drought across the western U.S. during the 15 months from December 2012 to March 2014.

We and Borsa et al. (2014) determine solid Earth's elastic response to a mass load to be nearly identical. We calculate solid Earth's elastic response for a gravitating, stratified sphere using the Green's function for PREM (Wang et al., 2012). Borsa et al. (2014) calculate solid Earth's elastic response in identical fashion except using the Green's function for the Gutenberg Bullen A Earth structure (Farrell, 1972). Solid Earth's elastic response to a 450 km $\times$ 60 km mass load differs by less than 4% between the two Earth structures (Figure 11, PREM is the blue curve; Gutenberg Bullen A is the green curve).

We and Borsa et al. (2014) differ in how we calculate vertical displacements attributable to water change. Borsa et al. (2014) determine vertical displacements on the basis of departures from the average vertical rate from 2006 to 2012. That is, they remove a vertical rate fit to the data at each GPS site then take the residual to be the elastic displacement produced by mass change. (Borsa et al., 2014 actually calculate the mean relative to the time period from 2003 to 2012. But because there are few data before 2006, this is effectively the mean from around 2006 to 2012.) In contrast, we assume vertical displacements produced by phenomena other than water change to be negligible (after removing GPS sites affected by groundwater change and volcanic activity). This method allows us to calculate water changes for all time periods, including that for drought from October 2006 to October 2009, that for heavy precipitation from October 2009 to October 2011, and that for drought from October 2011 to October 2015. Borsa et al. (2014) invert for water change for just

1 month, March 2014. In contrast, we determine a water series for each month from January 2006 to October 2017.

6.3. Product

We provide data files (see the acknowledgments) of this study's GPS estimates of change in total water storage as a function of location across the western U.S. each month from January 2006 to October 2017. Total mass can be separated into five components: (1) artificial reservoir surface water (CDEC), (2) atmosphere (ECMWF), (3) snow (SNODAS), (4) soil moisture (NLDAS Noah), and (5) other water (inferred to be groundwater or errors in the snow or soil moisture models).

Total water storage consists of snow, soil moisture, and other water. We are also providing estimates of change in total mass, equal to the sum of all five components. These estimates of mass change as a function of location are valuable to scientists determining fault stress changes produced by changes in snow and water. For example, Amos et al. (2014) and Johnson et al. (2017) find earthquakes occur more frequently when stress conditions due to seasonal snow and water changes are favorable to earthquake rupture.

7. Conclusions

7.1. Solid Earth's Elastic Response

Solid Earth's elastic response to a surface mass load must be evaluated using a gravitating, spherical model. Nongravitating, half-space models understate elastic vertical displacement by a factor of about 2.5.

Solid Earth's elastic response to changes in a mass load that is several tens of kilometers across is not very sensitive to Earth's structure. For example, for a 450 km × 60 km load (approximating the Central Valley), a stratified sphere with a sedimentary basin in the top 5 km (as in the deepest part of Los Angeles Basin) predicts elastic vertical displacement to be just 14% greater than a model with crystalline basement in the top 5 km.

7.2. Cause of Sierra Nevada Uplift

The Sierra Nevada rises during periods of drought and subsides during years of heavy precipitation. Because snow accumulation is insignificant in October, we quantify water changes and resulting elastic vertical displacement from October to October. Of the 24 mm of uplift of the Sierra Nevada during harsh drought from October 2011 to October 2015, just 5 mm is produced by unloading of Central Valley groundwater, less than 2 mm is tectonic uplift, and the remaining 17 mm is solid Earth's elastic response to water loss in the Sierra Nevada.

The southern Sierra Nevada has risen at a mean rate of about 1.5 mm/yr from January 2006 to December 2016. About 40% of this uplift is produced by unloading of Central Valley groundwater, up to 30% could be tectonic uplift, and the remaining 30–60% is solid Earth's elastic response to water loss in the Sierra Nevada (drought occurred in 7 of the 11 years of the time period).

7.3. Water Changes Sustained Over Periods of Drought and Years of Heavy Precipitation

Changes in total water storage in California's mountains ranges are sustained over periods of drought and years of heavy precipitation. The Sierra Nevada lost 15 ± 19 km^3 of water during drought from October 2006 to October 2009, gained 18 km ±14 km^3 of water during heavy precipitation from October 2009 to October 2011, and lost 45 ± 21 km^3 of water during severe drought from October 2011 to October 2015. (The values after the plus signs are realistic 95% confidence limits). The Sierra Nevada, Coast Ranges, and Klamath mountains lost a total of 97 ± 34 km^3 of water, yielding a mean increase in equivalent water thickness of 0.51 m. The drought caused the widespread death of trees in the Sierra Nevada (Asner et al., 2015; Potter, 2016).

7.4. Implications of Observation of Sustained Water Changes for Water-Balance Models: Parching and Seeping

Such sustained changes from October to October are absent in hydrology models. Hydrology models such as NLDAS and GLDAS consist of snow water equivalent and soil moisture. Snow accumulation is insignificant in October; change in soil moisture from October to October is small in the hydrology models. There must

therefore be large loss of deep soil moisture (absent in the hydrology models) or large loss of groundwater in river alluvium and in crystalline basement in the Sierra Nevada (not accounted for in the hydrology models).

Integration of the GPS inferences of changes in total water and the SNODAS snow model suggest that two water-balance processes (the parching of water from and the seeping of water into the ground) are occurring. In years of drought, all snow disappears in the spring and parching of the ground further reduces total water in the summer. In years of heavy precipitation, melting snow seeps into the Sierra Nevada in the spring, resulting in total water storage decreasing less quickly than snow mass.

Acknowledgments

Total water storage inferred from GPS in this study as a function of location each month from January 2006 to October 2017 are available by anonymous ftp at sideshow.jpl.nasa.gov in the directory /home/ftp/pub/usrs/argus/water/west.us; please contact donald.f.argus@jpl.nasa.gov for information. We are grateful to two anonymous reviewers, editor Paul Tregoning, Roland Burgmann, Kristel Chanard, and Manoo Shirzaei for constructive edits, suggestions, and criticism. We thank Claudia Faunt for the USGS CVHM model and Mu Xiao and Dennis Lettenmaier for the UCLA model of Central Valley groundwater change. NASA ROSES ESI 2013 supported this project. JPL's GPS team determined most of the position-time series in this study; Geoff Blewitt and Corne Kreemer at Nevada Geodetic Laboratory determined the remainder of the series. We are grateful to Greg Deemer at the National Snow and Ice Data Center and to Karl Tarbet at the U.S. Bureau of Reclamation for technical help on obtaining hydrologic data. This work was performed at the Jet Propulsion Laboratory, California Institute of Technology, under contract with NASA.

References

Amiri-Simkooei, A. R., Mohammadloo, T. H., & Argus, D. F. (2017). Multivariate analysis of GPS position time series of JPL's second reprocessing campaign. *Journal of Geodesy*, *91*(6), 685–704. https://doi.org/10.1007/s00190-016-0991-9

Amos, C. B., Audet, P., Hammond, W. C., Burgmann, R., Johanson, I. A., & Blewitt, G. (2014). Uplift and seismicity driven by groundwater depletion in central California. *Nature*, *509*(7501), 483–486. https://doi.org/10.1038/nature13275

Altamimi, Z., Collilieux, X., & Metivier, L. (2011). ITRF2008: An improved solution of the international terrestrial reference frame. *Journal of Geodesy*, *85*(8), 457–473. https://doi.org/10.1007/s00190-011-0444-4

Argus, D. F. (2007). Defining the translational velocity of the reference frame of Earth. *Geophysical Journal International*, *169*(3), 830–838. https://doi.org/10.1111/j.1365-246X.2007.03344.x

Argus, D. F. (2012). Uncertainty in the velocity between the mass center and surface of Earth. *Journal of Geophysical Research*, *117*, B10405. https://doi.org/10.1029/2012JB009196

Argus, D. F., Fu, Y., & Landerer, F. W. (2014). GPS as a high-resolution technique for evaluating water resources in California. *Geophysical Research Letters*, *41*, 1971–1980. https://doi.org/10.1002/2014GL059570

Argus, D. F., & Gordon, R. G. (2001). Present tectonic motion across the Coast Ranges and San Andreas fault system in central California. *Geological Society of America Bulletin*, *113*(12), 1580–1592. https://doi.org/10.1130/0016-7606(2001)113%3C1580:PTMATC%3E2.0.CO;2

Argus, D. F., Gordon, R. G., Heflin, M. B., Ma, C., Eanes, R. J., Willis, P., … Owen, S. E. (2010). The angular velocities of the plates and the velocity of Earth's center from space geodesy. *Geophysical Journal International*, *180*(3), 913–960. https://doi.org/10.1111/j.1365-246X.2009.04463.x

Argus, D. F., Peltier, W. R., Drummond, R., & Moore, A. W. (2014). The Antarctica component of postglacial rebound model ICE-6G_C (VM5a) based on GPS positioning, exposure age dating of ice thicknesses, and relative sea level histories. *Geophysical Journal International*, *198*(1), 537–563. https://doi.org/10.1093/gji/ggu140

Asner, G. P., Brodrick, P. B., Anderson, C. B., Vaughn, N., Knapp, D. E., & Martin, R. E. (2015). Progressive forest canopy loss during the 2012–2015 drought. *Proceedings of the National Academy of Sciences*, *113*(2), E249–E255. https://doi.org/10.1073/pnas.1523397113

Blewitt, G., Kreemer, C., Hammond, W. C., & Goldfarb, J. M. (2013). Terrestrial reference frame NA12 for crustal deformation studies in North America. *Journal of Geodynamics*, *72*, 11–24. https://doi.org/10.1016/j.jog.2013.08.004

Borsa, A. A., Agnew, D. C., & Cayan, D. R. (2014). Ongoing drought-induced uplift of the western United States. *Science*, *345*(6204), 1587–1590. https://doi.org/10.1126/science.1260279

California Data Exchange Center (CDEC) (2017a). Retrieved from http://cdec.water.ca.gov/snow_rain.html

California Data Exchange Center (CDEC) (2017b). Retrieved from http://cdec.water.ca.gov/resesrvoir.html

Cassel, E. J., Graham, S. A., & Chamberlain, C. P. (2009). Cenozoic tectonic and topographic evolution of the northern Sierra Nevada, California, through stable isotope paleoaltimetry in volcanic glass. *Geology*, *37*(6), 547–550. https://doi.org/10.1130/G25572A.1

Chanard, K., Avouac, J. P., Ramillien, G., & Genrich, J. (2014). Modeling deformation induced by seasonal variations of continental water in the Himalaya region: Sensitivity to Earth elastic structure. *Journal of Geophysical Research: Solid Earth*, *119*, 5097–5113. https://doi.org/10.1002/2013JB010451

Chang, W.-L., Smith, R. B., Farrell, J., & Puskas, C. M. (2010). An extraordinary episode of Yellowstone Caldera uplift, 2004–2010, from GPS and InSAR observations. *Geophysical Research Letters*, *37*, L23302. https://doi.org/10.1029/2010GL045451

Chaussard, E., Milillo, P., Burgmann, R., Perssin, D., Fielding, E. J., & Baker, B. (2017). Remote sensing of ground deformation for monitoring groundwater management practices: Applications to the Santa Clara Valley during the 2012–2015 drought. *Journal of Geophysical Research: Solid Earth*, *122*, 8556–8562. https://doi.org/10.1002/2017JB014676

Dee, D. P., Uppala, S. M., Simmons, A. J., Berrisford, P., Poli, P., Kobayashi, S., … Vitart, F. (2011). The ERA-Interim reanalysis: Configuration and performance of the data assimilation system. *Quarterly Journal of the Royal Meteorological Society*, *137*(656), 553–597. https://doi.org/10.1002/qj.828

Desai, S. D., Bertiger, W., Haines, B., Harvey, N., Kuang, D., Lane, C., … Weiss, J. (2011). Results from the reanalysis of the global GPS network, Fall 2009 AGU meeting G11B-0630.

Dmitrieva, K., Segall, P., & DeMets, C. (2015). Network-based estimation of time-dependent noise in GPS position time series. *Journal of Geodesy*, *89*(6), 591–606. https://doi.org/10.1007/s00190-015-0801-9

Dong, D., Qu, W., Fang, P., & Peng, D. (2014). Non-linearity of geocentre motion and its impact on the origin of the terrestrial reference frame. *Geophysical Journal International*, *198*(2), 1071–1080. https://doi.org/10.1093/gji/ggu187

D'Urso, M. G.,& Marmo, F. (2013). On a generalized Love's problem. *Computers and Geosciences*, *61*, 144–151. https://doi.org/20.1016/j.cageo.2013.09.002

Dziewonski, A. M., & Anderson, D. L. (1981). Preliminary reference Earth model. *Physics of the Earth and Planetary Interiors*, *25*(4), 297–356. https://doi.org/10.1016/0031-9201(81)90046-7

Dzurisin, D., Lisowski, M., Wicks, C. W., Poland, M. P., & Endo, E. T. (2006). Geodetic observations and modeling of magmatic inflation at the Three Sisters volcanic center, central Oregon Cascade Range, USA. *Journal of Volcanology and Geothermal Research*, *150*(1–3), 35–54. https://doi.org/10.1016/j.jvolgeores.2005.07.01

Famiglietti, J. S., Lo, M., Ho, S. L., Bethune, J., Anderson, K. J., Syed, T. H., … Rodell, M. (2011). Satellites measure recent rates of groundwater depletion in California's Central Valley. *Geophysical Research Letters*, *38*, L03403. https://doi.org/10.1029/2010GL046442

Farr, T. G., & Liu, Z. (2014). Monitoring subsidence associated with groundwater dynamics in the Central Valley of California using interferometric radar. In V. Lakshmi, et al. (Eds.), *Remote Sensing of the Terrestrial Water Cycle* (pp. 397–406). Hoboken, NJ: John Wiley, Inc. https://doi.org/10.1002/9781118872086.ch24

Farrell, W. E. (1972). Deformation of the Earth by surface loads. *Reviews of Geophysics*, *10*(3), 761–797. https://doi.org/10.1029/RG010i003p00761

Faunt, C. C. (Ed.) (2009). Groundwater availability of the Central Valley aquifer, California. U.S. Geological Survey professional paper 1766, Sacramento, CA.

Faunt, C. C., Sneed, M., Traum, J., & Brandt, J. T. (2015). Water availability and land subsidence in the Central Valley, California, USA (2015). *Hydrogeology Journal*, *24*(3), 675–684. https://doi.org/10.1007/s10040-015-1339-x

Forster, R. R. (2012). Evaluation of interferometric synthetic aperture radar (InSAR) techniques for measuring land subsidence and calculated subsidence rates for the Escalante Valley, Utah, 1998 to 2006, Open File Report 589, Utah Geological Survey.

Fu, Y., Argus, D. F., & Landerer, F. W. (2015). Seasonal and interannual variations of water storage in Washington and Oregon estimated from GPS measured surface loading deformation. *Journal of Geophysical Research: Solid Earth*, *120*, 552–566. https://doi.org/10.1002/2014JB011415

Gabet, E. J. (2014). Late Cenozoic uplift of the Sierra Nevada, California? A critical analysis of the geomorphic evidence. *American Journal of Science*, *314*(8), 1224–1257. https://doi.org/10.2475/08.2014.03

Griffin, D., & Anchukaitis, K. J. (2014). How unusual is the 2012–2014 California drought? *Geophysical Research Letters*, *41*, 9017–9023. https://doi.org/10.1002/2014GL062433

Hammond, W. C., Blewitt, G., Li, Z., Plag, H.-P., & Kreemer, C. (2012). Contemporary uplift of the Sierra Nevada, western United States, from GPS and InSAR measurements. *Geology*, *40*(7), 667–670. https://doi.org/10.1130/G32968

Hammond, W. C., Blewitt, G., & Kreemer, C. (2016). GPS imaging of vertical land motion in California and Nevada: Implications for Sierra Nevada uplift. *Journal of Geophysical Research: Solid Earth*, *121*, 7681–7703. https://doi.org/10.1029/2016JB013458

Jaeger, J. C., Cook, N. G. W., & Zimmerman, R. (2007). *Fundamentals of rock mechanics* (4th ed.). Malden, MA: Wiley-Blackwell.

Jiang, Y., Dixon, T. H., & Wdowinski, S. (2010). Accelerating uplift in the North Atlantic region as an indicator of ice loss. *Nature Geoscience*, *3*(6), 404–407. https://doi.org/10.1038/ngeo845

Johnson, C. W., Fu, Y., & Burgmann, R. (2017). Seasonal water storage, stress modulation, and California seismicity. *Science*, *356*(6343), 1161–1164. https://doi.org/10.1126/science.ask9547

Knudsen, T., Inkenbrandt, P., Lund, W., Lowe, M., & Bowman, S. (2014). Investigation of land subsidence and Earth fissures in Cedar Valley, Iron County, Utah, Special Study 150, Utah Geological Survey.

Landerer, F. W., & Swenson, S. C. (2012). Accuracy of scaled GRACE terrestrial water storage estimates. *Water Resources Research*, *48*, W04531. https://doi.org/10.1029/2011WR011453

Lawrence, D. M., Oleson, K. W., Flanner, M. G., Thornton, P. E., Swenson, S. C., Lawrence, P. J., … Slater, A. G. (2011). Parameterization improvements and functional and structural advances in version 4 of the Community Land Model. *Journal of Advances in Modeling Earth Systems*, *3*(3), M03001. https://doi.org/10.1029/2011MS000045

Le, K., Lee, J., Owen, L. A., & Finkel, R. (2007). Late Quaternary slip rates along the Sierra Nevada frontal fault zone, California: Slip partitioning across the western margin of the eastern California shear zone–Basin and Range Province. *Geological Society of America Bulletin*, *119*(1–2), 240–256. https://doi.org/10.1130/B25960

Luthcke, S. B., Sabaka, T. J., Loomis, B. D., Arendt, A. A., McCarthy, J. J., & Camp, J. (2013). Antarctica, Greenland, and Gulf of Alaska land-ice evolution from an iterated GRACE global mascon solution. *Journal of Glaciology*, *59*(216), 613–631. https://doi.org/10.3189/2013JoG12J147

McCaffrey, R., King, R. W., Payne, S. J., & Lancaster, M. (2013). Active tectonics of northwestern U.S. inferred from GPS-derived surface velocities. *Journal of Geophysical Research: Solid Earth*, *118*, 709–723. https://doi.org/10.1029/2012JB009473

Miller, M. M., & Shirzaei, M. (2015). Spatiotemporal characterization of land subsidence and uplift in Phoenix using InSAR time series and wavelet transforms. *Journal of Geophysical Research: Solid Earth*, *120*, 5822–5842. https://doi.org/10.1002/2015JB012017

Mitchell, K. E., Lohmann, D., Houser, P. R., Wood, E. F., Schaake, J. C., Robock, A., … Ramsay, B. H. (2004). The multi-institution North American Land Data Assimilation System (NLDAS): Utilizing multiple GCIP products and partners in a continental distributed hydrological modeling system. *Journal of Geophysical Research*, *109*, D07S90. https://doi.org/10.1029/2003JD003823

Montgomery-Brown, E. K., Wicks, C. W., Cervelli, P. F., Langbein, J. O., Svarc, J. L., Shelly, D. R., … Lisowski, M. (2015). Renewed inflation of Long Valley Caldera, California (2011 to 2014). *Geophysical Research Letters*, *42*, 5250–5257. https://doi.org/10.1002/2015GL064338

Mulch, A., Graham, S. A., & Chamberlain, P. C. (2006). Hydrogen isotopes in Eocene river gravels and paleoelevation of the Sierra Nevada. *Science*, *313*(5783), 87–89. https://doi.org/10.1126/science.1125986

Mulch, A., Graham, S. A., & Chamberlain, P. C. (2008). A Miocene to Pleistocene climate and elevation record of the Sierra Nevada (California). *Proceedings of the National Academy of Sciences*, *105*(19), 6819–6824. https://doi.org/10.1073/pnas.0708811105

National Hydrography Dataset (2017). Retrieved from https://nhd.usgs.gov/

National Operational Hydrologic Remote Sensing Center (2004). Snow Data Assimilation System (SNODAS) data products at NSIDC. Boulder, CO: National Snow and Ice Data Center. https://doi.org/10.7265/N5TB14TC

National Snow and Ice Data Center (2017). Retrieved from http://nsidc.org/data/docs/noaa/g02158_snodas_snow_cover_model/

Pan, M., Sheffield, J., Wood, E. F., Mitchell, K. E., Houser, P. R., Schaake, J. C., … Trapley, J. D. (2003). Snow process modeling in the North American Land Data Assimilation System (NLDAS): 2. Evaluation of model simulated snow water equivalent. *Journal of Geophysical Research*, *108*(D22), 8850. https://doi.org/10.1029/2003JD003994

Ouellette, K. J., de Linage, C., & Famiglietti, J. S. (2013). Estimating snow water equivalent from GPS vertical site-position observations in the western United States. *Water Resources Research*, *49*, 2508–2518. https://doi.org/10.1002/wrcr.20173

Parker, A. L., Biggs, J., & Lu, Z. (2016). Time-scale and mechanism of subsidence at Lassen Volcanic Center, CA, from InSAR. *Journal of Volcanology and Geothermal Research*, *158*(1–2), 37–50. https://doi.org/10.1016/j.jvolgeores.2006.04.013

Peltier, W. R., Argus, D. F., & Drummond, R. (2015). Space geodesy constrains ice age terminal deglaciation: The global ICE-6G_C (VM5a) model. *Journal of Geophysical Research: Solid Earth*, *120*, 450–487. https://doi.org/10.1002/2014JB011176

Petit, G., & Luzum, B. (Eds.) (2010). *IERS technical note 36* (179 pp.). Frankfurt, Germany: Bundesamts für Kartogr. und Geod.

Potter, C. S. (2016). Landsat image analysis of tree mortality in the southern Sierra Nevada region of California during the 2013–2015 drought. *Journal of Earth Science Climatic Change*, *07*(342), 1–7. https://doi.org/10.4172/2157-7617.1000342

Press, W. H., Teukolsky, S. A., Vetterling, W. T., & Flannery, B. P. (1992). *Numerical recipes in C, The art of scientific computing* (2nd ed.). Cambridge: Cambridge University Press.

PRISM Climate Group (2017). Northwest alliance for computation science and engineering, Oregon State University. Retrieved from http://www.prism.oregonstate.edu/

Riddell, A. R., King, M. A., Watson, C. S., Sun, Y., Riva, R. E. M., & Rietbroek, R. (2017). Uncertainty in geocenter estimates in the context of ITRF2014. *Journal of Geophysical Research: Solid Earth*, *122*, 4020–4032. https://doi.org/10.1002/2016JB013698

Rollins, C., Barbot, S., & Avouac, J.-P. (2015). Postseismic deformation following the 2010 *M* 7.2 El Mayor-Cucapah earthquake; Observations, kinematic inversions, and dynamic models. *Pure and Applied Geophysics*, *172*(5), 1305–1358. https://doi.org/10.1007/s00024-014-1005-6

Saleeby, J., Saleeby, Z., & Le Pourhiet, L. (2013). Epeirogenic transients related to mantle lithosphere removal in the southern Sierra Nevada region, California: Part II. Implications of rock uplift and basin subsidence relations. *Geosphere*, *9*(3), 394–425. https://doi.org/10.1130/GES00816.1

Save, H., Bettadpur, S., & Tapley, B. D. (2016). High resolution CSR GRACE RL05 Mascons. *Journal of Geophysical Research: Solid Earth*, *121*, 7547–7569. https://doi.org/10.1002/2016JB013007

Scanlon, B. R., Faunt, C. C., Longuevergne, L., Reedy, R. C., Alley, W. M., McGuire, V. L., & McMahon, P. B. (2012). Groundwater depletion and sustainability of irrigation in the U.S. high Plaines and Central Valley. *Proceedings of the National Academy of Sciences*, *109*(24), 9320–9325. https://doi.org/10.1073/pnas.1200311109

Schmid, R., Collilieux, X., Dilssner, F., Dach, R., & Schmitz, M. (2010). Updated phase center corrections for satellite and receiver antennas, June 2010 IGS workshop presentation, Newcastle, England.

Shaw, J. H., Plesch, A., Tape, C., Seuss, P. M., Jordan, T. H., Ely, G., … Munster, J. (2015). Unified structural representation of the southern California crust and upper mantle. *Earth and Planetary Science Letters*, *415*, 1–15. https://doi.org/10.1016/j.epsl.2015.01.016

Sibthorpe, A., Weiss, J. P., Harvey, N., Kuang, D., & Bar-Sever, Y. (2010). Empirical modeling of solar radiation pressure forces affecting GPS satellites. Abstract G54A-04 presented at 2010 Fall Meeting, AGU, San Francisco, Calif., 13–17 Dec.

Stock, G. M., Anderson, R. S., & Finkel, R. C. (2004). Pace of landscape evolution in the Sierra Nevada, California, revealed by cosmogenic dating of cave sediments. *Geology*, *32*(3), 193–196. https://doi.org/10.1130/G20197.1

Sneed, M., Brandt, J., & Solt, M. (2013). Land subsidence along the Delta-Mendota canal in the northern part of the San Joaquin Valley, California, 2003–10, *Scientific Investigations Report 2013–5142*, U.S. Geological Survey, Virginia.

Swain, D. L. (2015). A tale of two California droughts: Lessons amidst record warmth and dryness in region of complex physical and human geography. *Geophysical Research Letters*, *42*, 9999–10,003. https://doi.org/10.1002/2015GL066628

Thelin, G. P. and Pike, R. J. (1991). Landforms of the conterminous United States—A digital shaded-relief portrayal, U.S. Dept. Interior.

Tregoning, P., Watson, C., Ramillen, G., McQueen, H., & Zhang, J. (2009). Detecting hydrologic deformation using GRACE and GPS. *Geophysical Research Letters*, *36*, L15401. https://doi.org/10.1029/2009GL038718

Unruh, J. R. (1991). The uplift of the Sierra Nevada and implications for late Cenozoic epeirogeny in the western cordillera. *Geological Society of America Bulletin*, *103*, 395–1404. https://doi.org/10.1130/0016-7606

Wahr, J., Khan, S. A., van Dam, T., Liu, L., van Angelen, J. H., van den Broeke, M. R., & Meertens, C. M. (2013). The use of GPS horizontals for loading studies, with applications to northern California and southeast Greenland. *Journal of Geophysical Research: Solid Earth*, *118*, 1795–1806. https://doi.org/10.1002/jgrb.50104

Wahr, J., Molenaar, M., & Bryan, F. (1998). Time variability of the Earth's gravity field: Hydrological and oceanic effects and their possible detection using GRACE. *Journal of Geophysical Research*, *103*(B12), 30,205–30,229. https://doi.org/10.1029/98JB02844

Wakabayashi, J. (2013). Paleochannels, stream incision, erosion, topographic evolution, and alternative explanations of paleoaltimetry, Sierra Nevada, California. *Geosphere*, *9*(2), 191–215. https://doi.org/10.1130/GES00814

Wang, H., Xiang, L., Jia, L., Jiang, L., Wang, Z., Hu, B., & Gao, P. (2012). Load Love numbers and Green's functions for elastic Earth models PREM, iasp91, ak135, and modified models with refined crustal structure from crust 2.0. *Computational Geosciences*, *49*, 190–199. https://doi.org/10.1016/j.cageo.2012.06.022

Watkins, M. M., Wiese, D. N., Yuan, D.-N., Boening, C., & Landerer, F. W. (2015). Improved methods for observing Earth's time variable mass distribution with GRACE using spherical cap mascons. *Journal of Geophysical Research: Solid Earth*, *120*, 2648–2671. https://doi.org/10.1002/2014JB011547

Wesell, P., & Smith, W. H. F. (1998). New, improved version of Generic Mapping Tools released. *Eos, Transactions of the American Geophysical Union*, *79*(47), 579. https://doi.org/10.1029/98EO00426

Wicks, C. W., Thatcher, W., Dzurisin, D., & Svarc, S. (2006). Uplift, thermal unrest and magma intrusion at Yellowstone Caldera. *Nature*, *440*(7080), 72–75. https://doi.org/10.1038/nature04507

Wiese, D. N., Landerer, F. W., & Watkins, M. M. (2016). Quantifying and reducing leakage errors in the JPL RL05M GRACE mascon solution. *Water Resources Research*, *52*, 7490–7502. https://doi.org/10.1002/2016WR019344

Wiese, D. N., Yuan, D.-N., Boening, C., Landerer, F. W., & Watkins, M. M. (2017). JPL GRACE Mascon Ocean, ice, and hydrology equivalent water height RL05M.1 CRI filtered version 2., Ver. 2., PO.DAAC, CA. Retrieved from https://doi.org/10.5067/TEMSC-2LCR5

Xiao, M., Koppa, A., Mekonnen, Z., Pagan, B. R., Zhan, S., Cao, Q., … Lettenmaier, D. P. (2017). How much groundwater did California's Central Valley lose during the 2012–2016 drought? *Geophysical Research Letters*, *44*, 4872–4879. https://doi.org/10.1002/2017GL073333

Zumberge, J., Heflin, M., Jefferson, D., Watkins, M., & Webb, F. (1997). Precise point positioning for the efficient and robust analysis of GPS data from large networks. *Journal of Geophysical Research*, *102*(B3), 5005–5017. https://doi.org/10.1029/96jb03860